

Quantum many-body simulation of finite-temperature systems with sampling a series expansion of a quantum imaginary-time evolution

Norifumi Matsumoto,¹ Shoichiro Tsutsui,² Yuya O. Nakagawa,² Yuichiro Hidaka,²
Shota Kanasugi,¹ Kazunori Maruyama,¹ Hirotaka Oshima,¹ and Shintaro Sato¹

¹*Quantum Laboratory, Fujitsu Research, Fujitsu Limited.*

^{4-1-1 Kamikodanaka, Nakahara, Kawasaki, Kanagawa 211-8588, Japan}^{*}

²*QunaSys Inc., Aqua Hakusan Building 9F, 1-13-7 Hakusan, Bunkyo, Tokyo 113-0001, Japan*

(Dated: September 12, 2024)

Simulating thermal-equilibrium properties at finite temperature plays a crucial role in studying the nature of quantum many-body systems. In particular, implementing a finite-temperature simulation on a quantum computer is expected to overcome the difficulty in simulating large-sized systems, for which the quantum Monte-Carlo technique on a classical computer suffers from the sign problem in general. While several methods suitable for fault-tolerant quantum computing (FTQC) devices are expected to be useful in studying large-scale quantum many-body systems, those proposed so far involve a large number of ancilla qubits and a deep quantum circuit with many basic gates, making them unsuitable for the early-FTQC era, i.e., the early stage of the FTQC era, at which only a limited number of qubits and quantum gates are available. In this paper, we propose a method suitable for quantum devices in this early stage to calculate the thermal-equilibrium expectation value of an observable at finite temperature. Our proposal, named the Markov-chain Monte Carlo with sampled-pairs of unitaries (MCMC-SPU) algorithm, is based on sampling simple quantum circuits and generating the corresponding statistical ensembles, and overcomes the difficulties in the resource requirements and the decay in probability associated with postselection of measurement outcomes on ancilla qubits. We demonstrate the validity of our proposal by performing a numerical simulation of the MCMC-SPU algorithm on the one-dimensional transverse-field Ising model as an illustrative example.

I. INTRODUCTION

Recently, rapid progress in the technology of quantum control and quantum computing [1–3] has attracted widespread attention [4–8]. Among possible applications of quantum computers, one of the most promising candidates is the simulation of quantum many-body systems [4, 9–19], which plays a crucial role in various fields of science such as condensed-matter physics [9, 10, 12, 15], quantum chemistry [4, 10–13, 16, 18], and high-energy physics [10, 12, 14, 17, 19, 20]. In particular, one of the crucial tasks in quantum simulation is the evaluation of the ground-state energy of the system under consideration. For instance, the technique of the variational quantum eigensolver (VQE) [21–24] enables us to estimate the ground-state energy making use of near-term noisy intermediate-scale quantum (NISQ) devices [25–27]. Furthermore, the technique of the quantum phase estimation (QPE) [28–32] is believed to offer a more precise estimation of the ground-state energy on fault-tolerant quantum-computing (FTQC) devices.

Another important task in studying the nature of quantum many-body systems is the simulation of properties at finite temperature. To study finite-temperature properties, various techniques for classical computation have been established such as the quantum Monte-Carlo method [33–37], the minimally-entangled typical ther-

mal state (METTS) algorithm [38, 39], and the technique of the thermal pure quantum (TPQ) states [40–45]. In recent years, there have been proposals to implement finite-temperature-simulation techniques on quantum devices [46–51], and such implementation is expected to overcome the difficulty in simulating large-sized systems at finite temperature, for which the quantum Monte-Carlo technique on a classical computer suffers from the sign problem [52–54] in general. Furthermore, some of the proposals have been experimentally realized for small-sized systems [46, 48, 51, 55–58].

In the simulation of quantum many-body systems at finite temperature implemented on quantum devices, the quantum imaginary-time evolution (QITE) plays a crucial role in realizing the canonical statistical ensemble, also known as the Gibbs state (see Sec. II for details). For NISQ devices, the QITE is implemented by using techniques including variational methods [59–61], probabilistic methods [62, 63], and classical determination of coefficients in the Pauli decomposition [46], which has been studied in several experimental works [46, 55–57, 64–67]. While these methods suitable for NISQ devices have difficulty in scaling up, various techniques suitable for FTQC devices to implement the QITE have also been proposed and are expected to be useful in simulating large-scale systems. A representative one is the quantum eigenvalue/singular-value transformation (QET/QSVT) [68, 69], which involves the qubitization technique [70] and the quantum signal processing [71]. However, the latter fully utilizes quantum coherence, inevitably involving a large circuit depth, which leads to

* m.norifumi@fujitsu.com

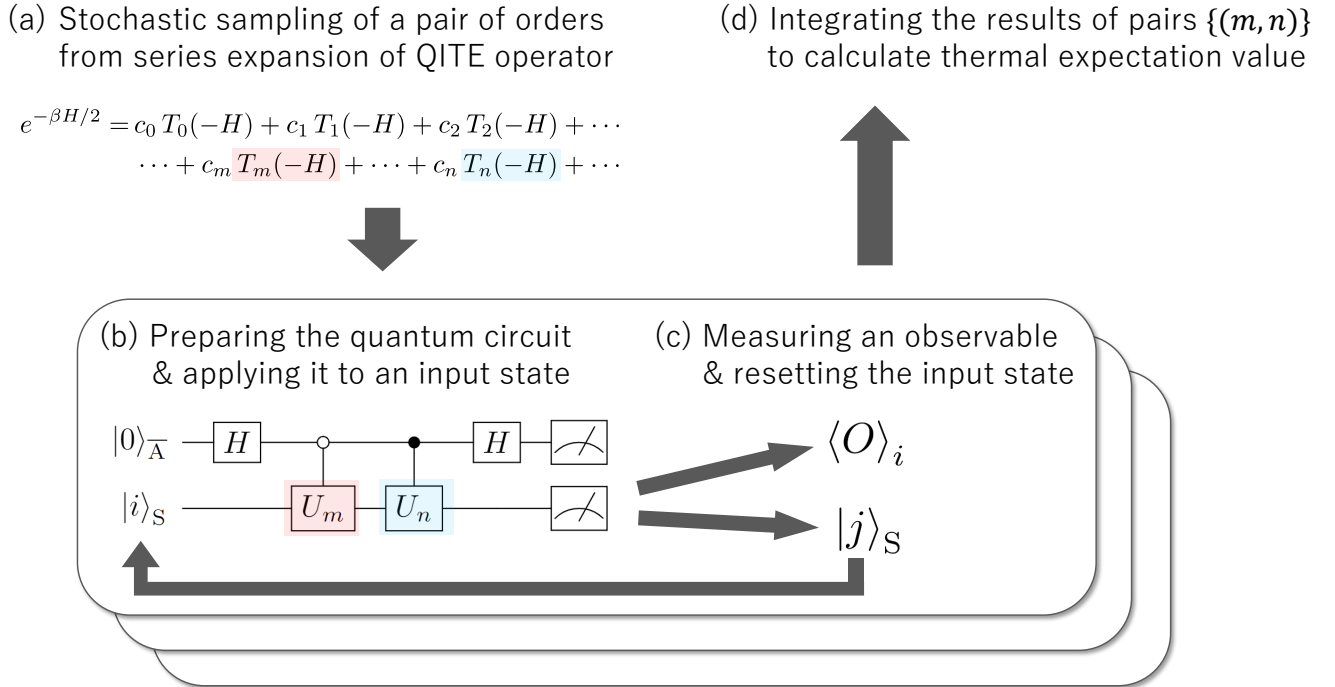


FIG. 1. Overview of our proposal of the Markov-chain Monte Carlo with sampled-pairs of unitaries (MCMC-SPU) algorithm. (a) Our proposal is based on a series expansion of a quantum imaginary-time evolution (QITE) operator. We perform stochastic sampling of a pair of orders m and n of polynomials from the series expansion. (b) For each pair of orders stochastically sampled in (a), we prepare a corresponding quantum circuit and apply it to a randomly chosen input state in the computational basis. (c) We measure an observable with respect to the state obtained in (b), and then reset the input state by performing a projective measurement on the output state of (b), the result of which is used as the input state for the next cycle. (d) We finally integrate the results of a large number of stochastic samples of pairs of orders m and n to calculate the thermal equilibrium expectation value of the observable at finite temperature.

difficulty in implementing at the early stage of the FTQC era (early-FTQC era).

Here, we focus on another representative method, the technique of the linear combination of unitaries (LCU) [72–76], since this method is free from the quantum signal processing and has flexibility in the form of the quantum circuit (see Sec. II B and II C for details). In the conventional form of the LCU method, the target matrix function such as an imaginary-time-evolution operator is expanded in some basis, each element of which is implemented with the corresponding controlled-unitary gate, and successive executions of such controlled-unitary gates result in a superposition of contributions of each element (see Sec. II B for details). In spite of the potential capability, however, the conventional form of the LCU technique involves a large number of ancilla qubits and a deep quantum circuit consisting of a large number of basic gates, and such implementation cost is unsuitable for early-FTQC devices [77–83], i.e., quantum devices available at the early-FTQC era, at which only a limited number of qubits and quantum gates are available. Furthermore, although there has been a recent proposal of the

single-ancilla LCU [84–88], which is an alternative implementation of the LCU suitable for the early-FTQC era involving simple quantum circuits (see Sec. II C for details), this proposal cannot be incorporated into the calculation of a finite-temperature observable in a straightforward manner. This is because the resulting state of the single-ancilla LCU is not the state after the QITE itself (see Sec. III for details).

In this paper, we propose a method suitable for early-FTQC devices to calculate the thermal-equilibrium expectation value of an observable at finite temperature. Our proposal, named the Markov-chain Monte Carlo with sampled-pairs of unitaries (MCMC-SPU) algorithm, is implemented with a set of simple quantum circuits and overcomes the difficulties involved with the conventional LCU implementation. Our MCMC-SPU is based on a series expansion of a QITE operator and a kind of Markov-chain Monte-Carlo (MCMC) sampling similar to that used in the METTS algorithm. We first perform a stochastic sampling of a pair of orders m and n of polynomials from the series expansion [Fig. 1 (a)]. For each pair of orders stochastically sampled, we prepare a cor-

responding quantum circuit and apply it to a randomly chosen input state in the computational basis [Fig. 1 (b)]. For the resulting state, we measure an observable and then perform a projective measurement in the computational basis on the output state of Fig. 1 (b), where the resulting state after the measurement is used as the input for the next cycle [Fig. 1 (c)]. We finally integrate the results of a large number of stochastic samples of pairs of orders m and n to calculate the thermal-equilibrium expectation value of the observable at finite temperature [Fig. 1 (d)]. In particular, the simple form of each quantum circuit with small depth [Fig. 1 (b)] makes our proposal well-suited for the early-FTQC era.

The rest of this paper is organized as follows. In Sec. II, as a preliminary, we present a review of some conventional techniques to calculate the thermal-equilibrium expectation value of an observable at finite temperature. In Sec. III, we introduce the MCMC-SPU algorithm. In Sec. IV, we discuss the implementation cost for the MCMC-SPU algorithm focusing on the number of qubits and quantum gates, the successful postselection probability, and the number of quantum circuits. As an illustrative example, we present a quantitative discussion focusing on the one-dimensional transverse-field Ising model. For the same model, we present a numerical demonstration of our MCMC-SPU algorithm in Sec. V. Finally, we present a discussion on our proposal and conclude this paper in Sec. VI.

II. REVIEW OF CONVENTIONAL TECHNIQUES

In this section, we present a review of some conventional techniques that form the basis of our method. We focus on the METTS algorithm [38, 39] as a prototypical method to calculate the thermal-equilibrium expectation value of an observable for a quantum many-body system at finite temperature. For a specific implementation of an imaginary-time evolution, which is a crucial part of the METTS algorithm, we review the LCU technique [72–76]. Furthermore, we discuss the technique of the single-ancilla LCU [84–88], which is a recently proposed implementation of the LCU algorithm suitable for early-FTQC devices with a limited number of qubits and quantum gates.

A. METTS algorithm

One representative method to calculate the thermal-equilibrium expectation value of an observable for a quantum many-body system at finite temperature is the METTS algorithm [38, 39]. In the standard framework of statistical mechanics, the thermal-equilibrium state of the target system coupled to a thermal bath at finite temperature is represented by the canonical statistical ensemble, also known as the Gibbs state. For this state, the

canonical ensemble average of an observable O is given by

$$\langle O \rangle_\beta = \frac{1}{Z} \text{Tr} [O e^{-\beta H}], \quad (1)$$

where β denotes the inverse temperature of the thermal bath to which the target system is coupled, and Z denotes the partition function

$$Z = \text{Tr} [e^{-\beta H}]. \quad (2)$$

In the computational basis $\{|i\rangle\}$, which consists of the classical product states (CPSs) $|i\rangle$'s, the canonical ensemble average in Eq. (1) for an N -qubit system can be rewritten as

$$\begin{aligned} \langle O \rangle_\beta &= \frac{1}{Z} \sum_{i=0}^{2^N-1} \langle i | e^{-(\beta/2)H} O e^{-(\beta/2)H} | i \rangle \\ &= \sum_{i=0}^{2^N-1} \frac{P_i}{Z} \langle \phi_i | O | \phi_i \rangle, \end{aligned} \quad (3)$$

where the normalized quantum state $|\phi_i\rangle$ corresponding to the CPS $|i\rangle$ is called the METTS [38, 39] with definition

$$|\phi_i\rangle := \frac{1}{P_i^{1/2}} e^{-(\beta/2)H} |i\rangle \quad (4)$$

and the normalization factor

$$P_i := \langle i | e^{-\beta H} | i \rangle. \quad (5)$$

The set of all the normalization factors P_i 's satisfy the following relation [see Eq. (2)]:

$$Z = \sum_{i=0}^{2^N-1} P_i. \quad (6)$$

The canonical ensemble average in Eq. (3) is obtained as the ensemble average of the observable O with respect to the statistical ensemble consisting of the set of the METTS $|\phi_i\rangle$'s with the probability distribution $\{P_i/Z\}$. The METTS algorithm [38, 39] generates this statistical ensemble consisting of a set of METTS as a stationary distribution of an MCMC sampling [89–92]. In the following, we present the concrete procedure of the METTS algorithm:

1. Choose a CPS $|i\rangle$ randomly from the computational basis.
2. Apply an imaginary-time evolution to the CPS $|i\rangle$ to obtain the corresponding METTS $|\phi_i\rangle$ as the resulting normalized state:

$$|i\rangle \rightarrow |\phi_i\rangle = \frac{1}{P_i^{1/2}} e^{-(\beta/2)H} |i\rangle. \quad (7)$$

3. Measure an observable O with respect to the METTS $|\phi_i\rangle$ to obtain its quantum-mechanical expectation value

$$\langle O \rangle_i = \langle \phi_i | O | \phi_i \rangle. \quad (8)$$

4. Collapse the METTS $|\phi_i\rangle$ onto some CPS $|j\rangle$ in the computational basis, i.e.,

$$|\phi_i\rangle \rightarrow |j\rangle \quad (9)$$

according to the probability $p(i \rightarrow j)$ given by the squared overlap between these states:

$$p(i \rightarrow j) = |\langle j | \phi_i \rangle|^2 = \frac{1}{P_i} \left| \langle j | e^{-(\beta/2)H} | i \rangle \right|^2. \quad (10)$$

The resulting state $|j\rangle$ is used as the input state for Step 2. [see Eq. (7)] in the next cycle, which is followed by Steps 3. and 4.

5. Calculate the statistical mean of the quantum-mechanical expectation values [see Eq. (8)] after many repetitions of cycles consisting of Steps 2.–4.

In particular, the quantum-mechanical expectation value (8) in Step 3. is obtained using an ensemble consisting of many copies of $|\phi_i\rangle$, and Step 4. is executed on an additional copy of the same state. While the METTS algorithm was originally proposed for calculation on a classical computer, a similar procedure can also be implemented on a quantum computer, and such implementation is referred to as the QMETTS in Refs. [46, 51, 55, 56, 93–97]. In the QMETTS algorithm, Step 2. in the above procedure is implemented by the QITE on a quantum computer, and Step 4. is naturally implemented via projective measurement in the computational basis.

One can confirm that the target distribution $\{P_i/Z\}$ satisfies the relation

$$\begin{aligned} \sum_{i=0}^{2^N-1} \frac{P_i}{Z} p(i \rightarrow j) &= \sum_{i=0}^{2^N-1} \frac{P_i}{Z} \frac{1}{P_i} \left| \langle j | e^{-(\beta/2)H} | i \rangle \right|^2 \\ &= \frac{P_j}{Z}. \end{aligned} \quad (11)$$

Therefore, if the process is irreducible, aperiodic, and positive, the target distribution is the stationary distribution of the Markov process $i \rightarrow j$ defined in Step 4. Thus, after the Markov process has converged, taking the statistical average of the expectation values (8) will yield the desired finite-temperature expectation value.

B. Linear combination of unitaries

As discussed in the previous subsection, implementing an imaginary-time evolution on a quantum device plays a crucial role in the QMETTS algorithm [see Eq. (7)].

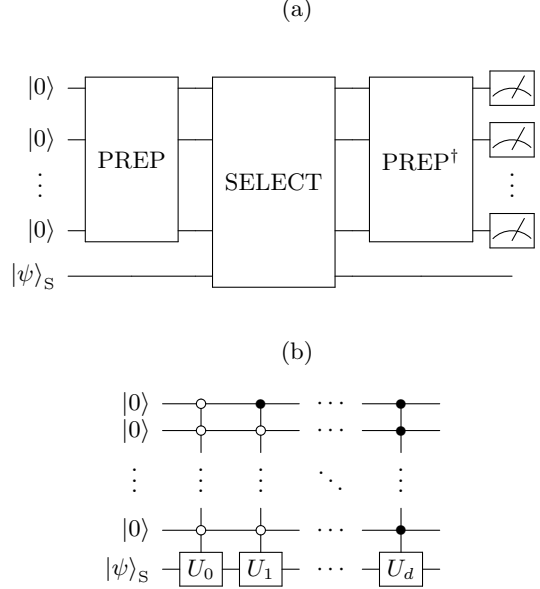


FIG. 2. Quantum circuit for the conventional form of the LCU technique. (a) A set of coefficients $\{c_k\}$ appearing in Eq. (12) is encoded in the ancilla qubits at the PREPARE circuit [see Eq. (13)], which is represented as a box with the label “PREP” in the figure. A series of unitary gates $\{U_k\}$ appearing in Eq. (12) are applied to the target state $|\psi\rangle_S$ successively at the SELECT circuit [see Eq. (14)], which is represented as a box with label “SELECT” in the figure. (b) Prototypical example of the implementation of the SELECT circuit, which takes the form of a series of multi-controlled unitary gates. The implementation can potentially be simplified depending on the specific form of $\{U_k\}$.

Among various methods of implementation proposed so far, we focus on the LCU technique [72–76] in this paper, since this method is free from the quantum signal processing [71] and flexible in implementation. In the following, we provide a brief overview of this technique. The LCU method is suitable for implementation on FTQC devices and is useful for implementing a variety of forms of matrix functions $f(M)$, where the argument is some matrix M . To implement such a matrix function on a quantum circuit, as shown in Fig. 2, we approximate the target function $f(M)$ by a linear combination of $(d+1)$ terms of simple unitary matrices $U_k(M)$ as follows:

$$f(M) \simeq \tilde{f}(M) = \sum_{k=0}^d c_k U_k(M), \quad (12)$$

where each unitary matrix $U_k(M)$ is a function of the matrix M and c_k denotes the corresponding real positive coefficient. A set of coefficients $\{c_k\}$ is encoded in ancilla qubits, which are initialized as a product of $|0\rangle$ states in Fig. 2, and each unitary matrix $U_k(M)$ is successively applied to the target system, which is represented as $|\psi\rangle_S$ in Fig. 2.

The encoding of the set of coefficients $\{c_k\}$ appearing in Eq. (12) into the ancilla qubits is implemented at the

PREPARE circuit [72], which is represented as the box with label ‘‘PREP’’ in Fig. 2(a). The action of the PREPARE circuit is given by

$$\text{PREP } |0\rangle_A = \sum_{k=0}^d \sqrt{\frac{c_k}{\sum_{k'=0}^d c_{k'}}} |k\rangle_A, \quad (13)$$

where $|0\rangle_A := |0\rangle^{\otimes \lceil \log_2(d+1) \rceil}$ and $|k\rangle_A$ ’s are multi-qubit ancilla states in the computational basis. Then a successive application of a series of unitary matrices $\{U_k(M)\}$ to the target state $|\psi\rangle_S$ is implemented at the SELECT circuit [72]. Specifically, a unitary gate $U_k(M)$ is applied to the target state $|\psi\rangle_S$ under the condition that the ancilla qubits are in the $|k\rangle_A$ state (see Fig. 2), i.e.,

$$\text{SELECT} = \sum_{k=0}^d |k\rangle_A \langle k| \otimes U_k(M). \quad (14)$$

A prototypical example of the implementation of the SELECT circuit is shown in Fig. 2(b), which takes the form of a series of multi-controlled unitary gates. The implementation can potentially be simplified depending on the specific form of $\{U_k\}$. Combining the SELECT circuit with the PREPARE circuit and its Hermitian conjugate, we approximately realize the desired matrix function $f(M) [\simeq \tilde{f}(M)]$ up to an overall constant factor as follows [see Fig. 2(a)]:

$$\begin{aligned} & (A\langle 0| \text{PREP}^\dagger) \cdot \text{SELECT} \cdot (\text{PREP } |0\rangle_A \otimes |\psi\rangle_S) \\ &= \frac{\tilde{f}(M)}{\sum_{k'=0}^d c_{k'}} |\psi\rangle_S, \end{aligned} \quad (15)$$

where the ancilla qubits are initialized as the $|0\rangle_A$ state. Here, after applying the PREP^\dagger , we perform a measurement on the ancilla qubits and make a postselection of the events where the measurement outcome is $|0\rangle_A$. Such postselection concerning the state of the ancilla qubits corresponds to restricting the action of the quantum circuit to a certain block element of the representation matrix, and this kind of implementation of a matrix function is called a block encoding [68, 98–101].

In the rest of Sec. II B, we discuss an LCU implementation of an imaginary-time evolution, which plays a crucial role in the QMETTS algorithm (see Sec. II A).

1. LCU implementation of an imaginary-time evolution

We first perform a decomposition of the imaginary-time-evolution operator. We employ an expansion based on a series of the Chebyshev polynomials $\{T_k(\cdot)\}$ as follows [86, 102, 103]:

$$e^{-(\beta/2)H} \simeq I_0(\beta/2) I + 2 \sum_{k=1}^d I_k(\beta/2) T_k(-H), \quad (16)$$

where $I_k(x)$ denotes the k -th order modified Bessel function of the first kind, which satisfies $I_k(x) > 0$ for $x > 0$, and the expansion is truncated up to the order d . In Eq. (16), the Hamiltonian H is normalized so that the absolute values of eigenenergies are equal or less than unity. In the LCU implementation, each of the series of matrix functions $T_k(-H)$ corresponds to $U_k(M)$ in the general form in Eq. (12). The specific implementation takes the form of the block encoding with a k -times iteration $(W_H)^k$ of the walk operator W_H [70, 103] combined with conditioning on the state of the ancilla qubits, i.e., [see Eq. (15)]

$$\begin{aligned} & (A\langle 0| \text{PREP}^\dagger) (W_H)^k (\text{PREP } |0\rangle_A \otimes |\psi\rangle_S) \\ &= T_k(-H) |\psi\rangle_S. \end{aligned} \quad (17)$$

The walk operator W_H itself can also be constructed on the basis of the LCU structure for the block encoding of the Hamiltonian H . In particular, in the case that the SELECT circuit SELECT_H for the block encoding of the Hamiltonian satisfies $(\text{SELECT}_H)^2 = I$, the walk operator can be obtained as [70, 103]

$$W_H = S_H \cdot \text{SELECT}_H \quad (18)$$

with the reflection S_H with respect to the ancilla state $\text{PREP}_H |0\rangle_{A,H}$, i.e.,

$$S_H = \text{PREP}_H \left(2 |0\rangle_{A,H} \langle 0| - I_A \right) \text{PREP}_H^\dagger \otimes I_S. \quad (19)$$

Here, PREP_H denotes the PREPARE circuit for the block encoding of the Hamiltonian and $|0\rangle_{A,H}$ denotes the product of $|0\rangle$ states of the corresponding ancilla qubits.

2. Successful postselection probability for quantum imaginary-time evolution

As discussed in Sec. II B, implementing a quantum imaginary-time evolution with the LCU technique involves measurement on the ancilla qubits and postselection of specific outcomes (see Eq. (15) and the following argument). In general, the probability of successful postselection decays exponentially with the value of the imaginary time or the inverse temperature β [104–107].

Specifically, for an initial state $|\psi\rangle = \sum_j \tilde{c}_j |E_j\rangle$, where $|E_j\rangle$ denotes the energy eigenstate with eigenenergy E_j , the unnormalized vector obtained as a result of a successful postselection for the LCU implementation of an imaginary-time evolution is given by [see Eqs. (15) and (16)]

$$\begin{aligned} |\psi(\beta/2)\rangle &\simeq \frac{e^{-(\beta/2)H}}{e^{\beta/2}} \sum_j \tilde{c}_j |E_j\rangle \\ &= \sum_j \tilde{c}_j e^{-(\beta/2)(E_j - E_{GS})} |E_j\rangle. \end{aligned} \quad (20)$$

Here, we assume that the eigenenergies are normalized as $-1 = E_{\text{GS}} < E_1 < \dots < E_j < \dots \leq 1$, as is the case in the argument for the expansion with the Chebyshev polynomials in Eq. (16). In Eq. (20), we have also used the relation $I_0(\beta/2) + 2 \sum_{k=1}^d I_k(\beta/2) \simeq e^{\beta/2}$ for a sufficiently large value of d [86] (see Eqs. (46) and (49) in Sec. IV for details). The probability of a successful postselection of the measurement outcome on the ancilla qubits is proportional to the squared norm of the unnormalized vector in Eq. (20), which satisfies

$$p_{\text{PS}} \propto \langle \psi(\beta/2) | \psi(\beta/2) \rangle \geq e^{-2\beta}. \quad (21)$$

In this evaluation, we have used the relation $\langle \psi(\beta/2) | \psi(\beta/2) \rangle \simeq \sum_j |\tilde{c}_j|^2 e^{-\beta(E_j+1)}$ together with the normalization condition $\sum_j |\tilde{c}_j|^2 = 1$. From Eq. (21), the number of trials N_{PS} required to ensure that we obtain a successful measurement outcome for general models scales as $N_{\text{PS}} = \mathcal{O}(e^{2\beta})$ in the worst case (see also Ref. [108]).

C. Single-ancilla LCU

The conventional form of the LCU algorithm discussed in Sec. II B involves many ancilla qubits and a deep quantum circuit consisting of a large number of basic gates, which is unsuitable for the early stage of the FTQC regime (see Figs. 5(a)–(c) for an illustrative example). Recently, there has been a proposal [84–88] of a variant form of the LCU method involving a set of simple quantum circuits as shown in Fig. 3 at the cost of the statistical sampling overhead (see also Sec. IV C). In particular, in Ref. [85], this form of implementation is named “single-ancilla LCU” after the structure of the quantum circuits. In the following, we present a brief review of this method.

We focus on a certain form [84–88] of the single-ancilla LCU, which can be used to estimate the expectation value $\langle O \rangle_{f(M)}$ of an observable O with respect to the resulting unnormalized state $f(M) |\psi\rangle_S$ after applying a matrix function $f(M)$ to the initial state $|\psi\rangle_S$, i.e.,

$$\langle O \rangle_{f(M)} = \langle \psi | f(M) O f(M) | \psi \rangle. \quad (22)$$

Applying the LCU decomposition in Eq. (12) to this equation, $\langle O \rangle_{f(M)}$ is approximated by

$$\begin{aligned} \langle O \rangle_{\tilde{f}(M)} &= \sum_{m=0}^d \sum_{n=0}^d c_m c_n \text{s} \langle \psi | U_m^\dagger(M) O U_n(M) | \psi \rangle_S \\ &= \sum_{m=0}^d \sum_{n=0}^d p_m p_n \|c\|_1^2 \text{s} \langle \psi | U_m^\dagger(M) O U_n(M) | \psi \rangle_S, \end{aligned} \quad (23)$$

where we have introduced the following notations: $\|c\|_1 = \sum_{n=0}^d c_n$ and $p_n = c_n / \|c\|_1$. Here, for the d -th-order approximation $\tilde{f}(\cdot)$ of $f(\cdot)$ satisfying Eq. (46), the

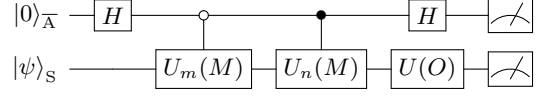


FIG. 3. Quantum circuit for the single-ancilla LCU. The circuit consists of a pair of unitary gates $U_m(M)$ and $U_n(M)$, which are stochastically sampled from the set of the unitary gates $\{U_0(M), U_1(M), \dots, U_d(M)\}$ appearing in the conventional LCU method (see Fig. 2). In contrast to the conventional implementation, the quantum circuit in this implementation involves a single ancilla qubit, which plays a role of the control degree of freedom for the controlled unitary gates. After applying the circuit to the initial state $|0\rangle_{\text{A-bar}} \otimes |\psi\rangle_S$, we perform a simultaneous measurement of the Pauli Z operator of the ancilla qubit and a general observable O for the target system, the latter of which is implemented with some unitary gate $U(O)$. By calculating the statistical mean of the results for various pairs of unitary gates that are stochastically sampled, we can reproduce the result of the original LCU method.

approximation error in the observable is upper bounded as [86]

$$|\langle O \rangle_{\tilde{f}(M)} - \langle O \rangle_{f(M)}| \leq \nu \|O\|_{\text{op}} (2\|f(M)\|_{\text{op}} + \nu) \quad (24)$$

with operator norm $\|\cdot\|_{\text{op}}$. The quantity on the right-hand side of Eq. (23) can be obtained by stochastically sampling a pair of unitary gates U_m and U_n according to the probability distribution $\{p_n\}$ and by calculating the value of a stochastic variable $\|c\|_1^2 \text{s} \langle \psi | U_m^\dagger(M) O U_n(M) | \psi \rangle_S$. The quantity $\text{s} \langle \psi | U_m^\dagger(M) O U_n(M) | \psi \rangle_S$ can be obtained using the quantum circuit shown in Fig. 3, which consists of the stochastically sampled pair of unitary gates $U_m(M)$ and $U_n(M)$. In contrast to the conventional implementation (see Fig. 2), the quantum circuit in this implementation involves a single ancilla qubit. The state after applying the quantum circuit to the initial state $|0\rangle_{\text{A-bar}} \otimes |\psi\rangle_S$ is given by

$$|0\rangle_{\text{A-bar}} \otimes \frac{1}{2}(U_m + U_n) |\psi\rangle_S + |1\rangle_{\text{A-bar}} \otimes \frac{1}{2}(U_m - U_n) |\psi\rangle_S. \quad (25)$$

For this state, we evaluate the expectation value $\langle O \rangle_{mn}^0$ ($\langle O \rangle_{mn}^1$) of an observable O for the target system under the condition that the outcome of a simultaneous measurement on the ancilla qubit is 0 (1) as follows:

$$\langle O \rangle_{mn}^0 = \frac{1}{4} \text{s} \langle \psi | (U_m^\dagger + U_n^\dagger) O (U_m + U_n) | \psi \rangle_S, \quad (26)$$

$$\langle O \rangle_{mn}^1 = \frac{1}{4} \text{s} \langle \psi | (U_m^\dagger - U_n^\dagger) O (U_m - U_n) | \psi \rangle_S. \quad (27)$$

From these equations, we obtain the desired quantity as

$$\begin{aligned} \langle O \rangle_{mn}^0 - \langle O \rangle_{mn}^1 &= \frac{1}{2} \text{s} \langle \psi | (U_m^\dagger O U_n + U_n^\dagger O U_m) | \psi \rangle_S \\ &= \text{Re} [\text{s} \langle \psi | U_m^\dagger O U_n | \psi \rangle_S], \end{aligned} \quad (28)$$

which is sufficient to evaluate the quantity on the right-hand side of Eq. (23), since a stochastic sampling of a pair of (m, n) and that of (n, m) are equivalent and thus only the real part of each term contributes to the summation.

III. MARKOV-CHAIN MONTE CARLO WITH SAMPLED PAIRS OF UNITARIES

As discussed in the previous section, the single-ancilla LCU is suitable for the early-FTQC era for implementing a quantum imaginary-time evolution (see Sec. II C), which plays a crucial role in a simulation of finite-temperature quantum many-body systems (see Sec. II A). However, the state obtained after applying a quantum circuit in the single-ancilla LCU [see Eq. (25)] is not the METTS itself in Eq. (4), indicating that QITE in the QMETTS algorithm cannot be replaced with the single-ancilla LCU in a straightforward manner.

In this section, we propose the MCMC-SPU algorithm (see Fig. 1). This algorithm is suitable for the early-FTQC era to calculate the thermal-equilibrium expectation value of an observable at finite temperature. Our proposal is based on a kind of MCMC sampling to generate a statistical ensemble corresponding to each quantum circuit (see Fig. 4) appearing in the single-ancilla-LCU implementation of a quantum imaginary-time evolution.

A. Procedure of the MCMC-SPU algorithm

In the following, we present a concrete procedure for our MCMC-SPU algorithm. Our proposal is based on a quantum imaginary-time evolution [see Eq. (16)] implemented with the single-ancilla-LCU method (see Sec. II C).

1. Sample a pair of orders m and n of the Chebychev polynomials in Eq. (16) in a stochastic manner according to the probability distribution $\{p_n = c_n / (\sum_{n'=0}^d c_{n'})\}$, where the coefficient c_n is given by

$$c_n = \begin{cases} I_0(\beta/2) & (n = 0); \\ 2I_n(\beta/2) & (n \neq 0). \end{cases} \quad (29)$$

2. Construct a quantum circuit U_{mn} given by Fig. 4(b), which corresponds to the sampled pair of orders m and n . In Fig. 4(b), $(W_H)^{m(n)}$ denotes the $m(n)$ -times iteration of the walk operator W_H [see Eq. (18)] forming the block encoding of the $m(n)$ -th order Chebyshev polynomial.
3. Prepare an initial state

$$|i\rangle_{\text{tot}} := |0\rangle_{\bar{A}} \otimes |G\rangle_A \otimes |i\rangle_S, \quad (30)$$

where $|i\rangle_S$ denotes a CPS randomly chosen from the computational basis for the target system. Here,

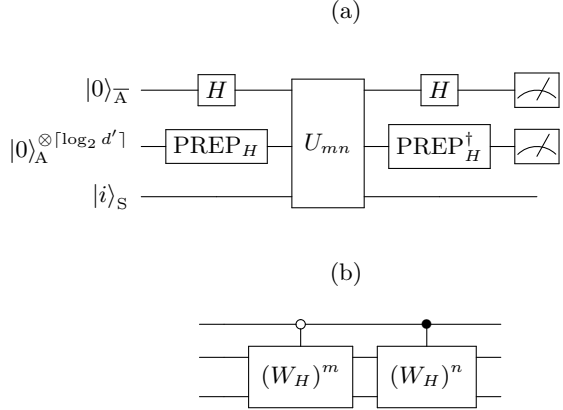


FIG. 4. (a) Quantum circuit for our proposal of the MCMC-SPU. The specific form of the gate U_{mn} is given in (b), which corresponds to a sampled pair of orders m and n . In Fig. (b), each box represents the $m(n)$ -times iteration $(W_H)^{m(n)}$ of the walk operator W_H [see Eq. (18)] forming the block encoding of the $m(n)$ -th-order Chebyshev polynomial. The ancilla state $|G\rangle_A = \text{PREP}_H |0\rangle_A^{\otimes \lceil \log_2 d' \rceil}$ is prepared with the PREPARE circuit PREP_H for the block encoding of the Hamiltonian H consisting of d' terms, while $|i\rangle_S$ denotes the target system in the computational basis.

$|0\rangle_{\bar{A}}$ denotes an ancilla qubit which plays the role of the control qubit for $(W_H)^m$ and $(W_H)^n$, and the ancilla state $|G\rangle_A = \text{PREP}_H |0\rangle_A^{\otimes \lceil \log_2 d' \rceil}$ is prepared with PREP_H [see Fig. 4(a)], which is a specific form of the PREPARE circuit (see Eq. (13) for the general form) for the block encoding of the Hamiltonian H .

4. Apply the quantum circuit U_{mn} shown in Fig. 4(b) to the initial state in Eq. (30), and then apply PREP_H^\dagger to the ancilla qubits.
5. Perform measurement on the ancilla qubits in the computational basis, and make postselection of measurement outcome of the ancilla qubits with the result $|k\rangle_{\bar{A}} \otimes |0\rangle_A^{\otimes \lceil \log_2 d' \rceil}$ for $k \in \{0, 1\}$, which results in projection onto a normalized state $|\phi_{mn}^{ik}\rangle$ (see Eq. (33) in Sec. III B for details).
6. Perform a measurement of an observable O with respect to the resulting state $|\phi_{mn}^{ik}\rangle$ to obtain its quantum-mechanical expectation value

$$\langle O \rangle_{mn}^{ik} = \langle \phi_{mn}^{ik} | O | \phi_{mn}^{ik} \rangle. \quad (31)$$

Evaluating this expectation value is executed with an ensemble consisting of many copies of $|\phi_{mn}^{ik}\rangle$.

7. Collapse an additional copy of the state $|\phi_{mn}^{ik}\rangle$ onto some CPS $|j\rangle_S$ in the computational basis for the target system by performing projective measurement on the target system. A transition $|\phi_{mn}^{ik}\rangle \rightarrow |j\rangle_S$ realizes with probability $|S\langle j|\phi_{mn}^{ik}\rangle|^2$

(see Eq. (42) in Sec. III B for details). The resulting state $|j\rangle_S$ is used as the input state for Step 3. [see Eq. (30)] in the next cycle, which is followed by Steps 4–6.

8. Calculate the statistical mean $\langle O \rangle_{mn}^k$ (see Eq. (40) for the definition) of the quantum-mechanical expectation values in Eq. (31) after a large number of repetitions of cycles consisting of Steps 3–7.
9. Repeat Steps 1–8. many times with resampling a pair of orders m and n for each cycle, and then calculate the statistical ensemble average of $\{\langle O \rangle_{mn}^k\}$ with an appropriately-defined weight (see Eqs. (37)–(40) in the following).

B. Validity of the MCMC-SPU algorithm

We now present the proof of the validity of the MCMC-SPU algorithm. In Step 5. in Sec. III A, the resulting unnormalized vector after measurement on the ancilla qubits is given by (see Fig. 4)

$$\begin{aligned} & (\langle k|_{\bar{A}} \otimes \langle G|_A) U_{mn} |i\rangle_{\text{tot}} \\ &= \frac{1}{\sqrt{2}} [T_m(-H) + (-1)^k T_n(-H)] |i\rangle_S, \end{aligned} \quad (32)$$

from which we obtain the corresponding normalized state vector

$$|\phi_{mn}^{ik}\rangle := \frac{1}{\sqrt{W_{mn}^{ik}}} (\langle k|_{\bar{A}} \otimes \langle G|_A) U_{mn} |i\rangle_{\text{tot}} \quad (33)$$

with probability of successful postselection, which is given by

$$W_{mn}^{ik} := \text{tot}\langle i| U_{mn}^\dagger (|k\rangle_{\bar{A}} \otimes |G\rangle G \otimes I_S) U_{mn} |i\rangle_{\text{tot}}. \quad (34)$$

The value of W_{mn}^{ik} is real nonnegative since it is the expectation value of a projection operator. In particular, it follows from Eq. (32) that

$$\langle (1|_{\bar{A}} \otimes \langle G|_A) U_{mm} |i\rangle_{\text{tot}} = 0. \quad (35)$$

This fact means that the pair of orders (m, n) with $m = n$ and $k = 1$ has no contribution to the finite-temperature observable, and thus we skip Steps 2–8. for these combinations of indices. On the basis of the relation in Eq. (32), the thermal expectation value of an observable O can be expressed in terms of its quantum-mechanical expectation value for the normalized states $|\phi_{mn}^{ik}\rangle$'s as

$$\langle O \rangle_\beta \simeq \frac{\sum_{m,n=0}^d \sum_i c_m c_n \text{S}\langle i| T_m(-H) O T_n(-H) |i\rangle_S}{\sum_{m',n'=0}^d \sum_{i'} c_{m'} c_{n'} \text{S}\langle i'| T_{m'}(-H) T_{n'}(-H) |i'\rangle_S} \quad (36)$$

$$= \frac{\sum_{m,n} p_m p_n \sum_{k=0}^1 (-1)^k 2^{-N} \sum_i W_{mn}^{ik} \langle \phi_{mn}^{ik} | O | \phi_{mn}^{ik} \rangle}{\sum_{m',n'} p_{m'} p_{n'} \sum_{k'=0}^1 (-1)^{k'} 2^{-N} \sum_{i'} W_{m'n'}^{i'k'}}, \quad (37)$$

which is the counterpart of Eq. (3) in the METTS algorithm. From the relation in Eq. (37), the thermal expectation value $\langle O \rangle_\beta$ can be obtained as a weighted average of the quantity $2^{-N} \sum_{i=0}^{2^N-1} W_{mn}^{ik} \langle \phi_{mn}^{ik} | O | \phi_{mn}^{ik} \rangle$ with respect to sampling of pairs of orders m and n , which is realized in Step 9. in Sec. III A. The quantity appearing in the numerator on the right-hand side of Eq. (37) can be rewritten as

$$2^{-N} \sum_{i=0}^{2^N-1} W_{mn}^{ik} \langle \phi_{mn}^{ik} | O | \phi_{mn}^{ik} \rangle = (2^{-N} Z_{mn}^k) \langle O \rangle_{mn}^k, \quad (38)$$

where Z_{mn}^k on the right-hand side is given by

$$Z_{mn}^k := \sum_{i=0}^{2^N-1} W_{mn}^{ik}, \quad (39)$$

and the corresponding quantity $\langle O \rangle_{mn}^k$ is defined as

$$\langle O \rangle_{mn}^k := \sum_{i=0}^{2^N-1} \frac{W_{mn}^{ik}}{Z_{mn}^k} \langle \phi_{mn}^{ik} | O | \phi_{mn}^{ik} \rangle. \quad (40)$$

The weight factor $2^{-N} Z_{mn}^k = 2^{-N} \sum_{i=0}^{2^N-1} W_{mn}^{ik}$ on the right-hand side of Eq. (38) and the denominator in Eq. (37) can be obtained as a statistical mean of $\{W_{mn}^{ik}\}$ evaluated by uniform sampling with respect to the label i (see Appendix A for a discussion on the efficiency of this sampling). The value of W_{mn}^{ik} can be evaluated as the probability of obtaining the measurement outcome of the ancilla qubits with the result $|k\rangle_{\bar{A}} \otimes |0\rangle_A^{\otimes \lceil \log_2 d' \rceil}$ in Step 5. of the procedure in Sec. III A. The quantity $\langle O \rangle_{mn}^k$ in Eq. (40) can be evaluated as the ensemble average of the observable O with respect to the statistical ensemble consisting of the set of states $\{|\phi_{mn}^{ik}\rangle\}$ with the probability distribution $\{W_{mn}^{ik}/Z_{mn}^k\}$.

As shown in the following, the probability distribution $\{W_{mn}^{ik}/Z_{mn}^k\}$ can be obtained as a stationary distribution of the Markov process $i \rightarrow j$ with respect to the label of states of the target system in the computational basis, where the Markov process is defined by Step 7. in the procedure in Sec. III A. Indeed, if we begin with the probability distribution $\{W_{mn}^{ik}/Z_{mn}^k\}$, the resulting probability for the label j after one step of this Markov process is shown to be obtained as

$$\sum_{i=0}^{2^N-1} \frac{W_{mn}^{ik}}{Z_{mn}^k} |\text{S}\langle j| \phi_{mn}^{ik} \rangle|^2 = \frac{W_{mn}^{jk}}{Z_{mn}^k}. \quad (41)$$

To see this, we note that the transition probability from

the label i to j in this Markov process is given by

$$\begin{aligned} & |\langle s|j|\phi_{mn}^{ik}\rangle|^2 \\ &= \frac{1}{W_{mn}^{ik}} \text{tot} \langle i| U_{mn}^\dagger (|k\rangle\langle k|_{\bar{A}} \otimes |G\rangle\langle G|_A \otimes |j\rangle\langle j|_S) U_{mn} |i\rangle_{\text{tot}} \\ &= \frac{1}{W_{mn}^{ik}} \text{tot} \langle j| U_{mn}^\dagger (|k\rangle\langle k|_{\bar{A}} \otimes |G\rangle\langle G|_A \otimes |i\rangle\langle i|_S) U_{mn} |j\rangle_{\text{tot}}. \end{aligned} \quad (42)$$

In this transformation, we have used the Hermiticity of the block element of the representation matrix for the whole quantum circuit conditioned on the measurement outcomes on the ancilla qubits, i.e.,

$$\begin{aligned} & \bar{A} \langle k| \otimes {}_A\langle G| \otimes {}_S\langle j| U_{mn} |0\rangle_{\bar{A}} \otimes |G\rangle_A \otimes |i\rangle_S \\ &= {}_S\langle j| (\bar{A} \langle k| \otimes {}_A\langle G| U_{mn} |0\rangle_{\bar{A}} \otimes |G\rangle_A)^\dagger |i\rangle_S \\ &= \bar{A} \langle 0| \otimes {}_A\langle G| \otimes {}_S\langle j| U_{mn}^\dagger |k\rangle_{\bar{A}} \otimes |G\rangle_A \otimes |i\rangle_S. \end{aligned} \quad (43)$$

On the basis of the above observation, we can show Eq. (41) as

$$\begin{aligned} & \sum_{i=0}^{2^N-1} \frac{W_{mn}^{ik}}{Z_{mn}^k} |\langle j|\phi_{mn}^{ik}\rangle|^2 \\ &= \frac{1}{Z_{mn}^k} \text{tot} \langle j| U_{mn}^\dagger (|k\rangle\langle k|_{\bar{A}} \otimes |G\rangle\langle G|_A \otimes I_S) U_{mn} |j\rangle_{\text{tot}} \\ &= \frac{W_{mn}^{jk}}{Z_{mn}^k}, \end{aligned} \quad (44)$$

which confirms that $\{W_{mn}^{ik}/Z_{mn}^k\}$ is a stationary distribution of the Markov process. From this result, a large number of repetitions of cycles consisting of Steps 3.-7. result in the evaluation of Eq. (40), which leads to the calculation of a finite-temperature expectation value of an observable via Eq. (37).

IV. IMPLEMENTATION COST FOR THE MCMC-SPU ALGORITHM

In this section, we discuss the implementation cost of the MCMC-SPU algorithm focusing on the number of qubits, quantum gates, and quantum circuits, as well as the successful postselection probability with respect to the measurement outcome of the ancilla qubits. As an illustrative example, we consider the one-dimensional transversal-field Ising model with the Hamiltonian

$$H_{\text{TFI}} = \sum_{j=1}^N J \sigma_j^x \sigma_{j+1}^x + h \sigma_j^y. \quad (45)$$

We parameterize the coefficients as $J = N^{-1} \cos^2(\theta/2)$ and $h = N^{-1} \sin^2(\theta/2)$ with a single parameter θ . This parameterization arises naturally in the LCU implementation of the block encoding.

A. Number of qubits and quantum gates

We first discuss the number of qubits and quantum gates required for implementing each quantum circuit appearing in the MCMC-SPU algorithm. The required resources depend on the truncation order d of the LCU method [see Eq. (16)]. The order d is determined by the inverse temperature β at which we perform a simulation and by the precision ν of the approximation. Specifically, to ensure that the d -th order approximation $\tilde{f}(\cdot)$ of $f(\cdot)$ satisfies

$$\max_{x \in \text{Dom}(f)} |f(x) - \tilde{f}(x)| \leq \nu \quad (46)$$

with the domain $\text{Dom}(f)$ of $f(\cdot)$, the required truncation order of LCU is given by [86, 109]

$$d = \sqrt{2 \log\left(\frac{4e^{\beta/2}}{\nu}\right) \cdot \max\left[\frac{e^2\beta}{2}, \log\left(\frac{2e^{\beta/2}}{\nu}\right)\right]} \quad (47)$$

xhibiting a nearly linear scaling with β [see also Eq. (24)]. By contrast, in stochastically sampling pairs (m, n) of orders with $m \leq d$ and $n \leq d$ in the MCMC-SPU algorithm (see Step 1. in Sec. III A), the weighted average d_{average} of a sampled value of order n is evaluated as [86]

$$\begin{aligned} d_{\text{average}} &= \frac{1}{\|c\|_1} \sum_{n=1}^d n c_n \simeq e^{-\beta/2} \sum_{n=1}^d 2n I_n(\beta/2) \\ &\leq \frac{\beta}{2} e^{-\beta/2} [I_0(\beta/2) + I_1(\beta/2) - I_d(\beta/2) - I_{d+1}(\beta/2)], \end{aligned} \quad (48)$$

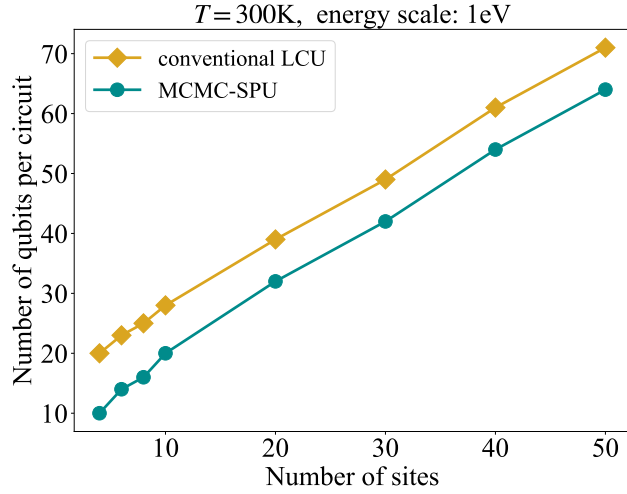
the most right-hand side of which exhibits a scaling $\mathcal{O}(\sqrt{\beta})$ as $\beta \rightarrow \infty$. In this transformation, we have used the relations $n I_n(\beta/2) = (\beta/4)[I_{n-1}(\beta/2) - I_{n+1}(\beta/2)]$ and

$$|||c||_1 - e^{\beta/2}| \leq \nu \quad (49)$$

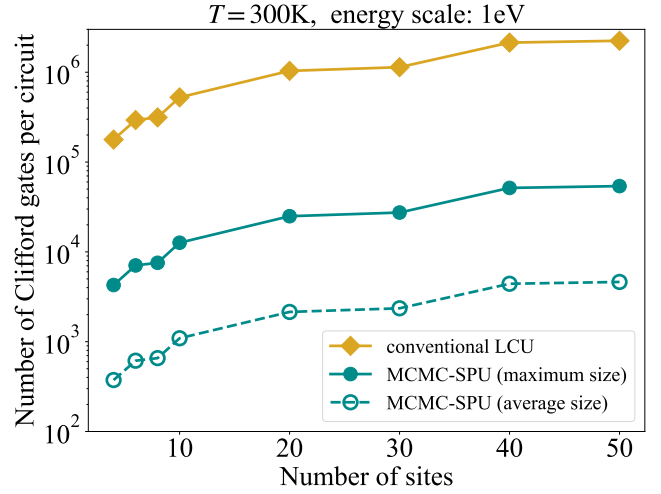
with a sufficiently small value of ν [86]. The difference in scaling behavior between d and d_{average} as $\beta \rightarrow \infty$ presents a significant advantage of stochastic sampling, leading to a significant reduction in implementation resources [86] in our MCMC-SPU algorithm. Note that our MCMC-SPU algorithm involves the sampling overhead as discussed in Sec. IV C.

The truncation order d of the LCU method in Eq. (47) determines the required resource for implementing each quantum circuit through sampled values of orders of the polynomials appearing in the series expansion in Eq. (16). Each polynomial is implemented with $(W_H)^k$ via Eq. (17) with W_H given by Eq. (18) with Eq. (19), which leads to the number of qubits and the gate count of each quantum circuit. The concrete form of W_H depends on the Hamiltonian. In our specific implementation, PREP_H in Eq. (19) for an N -site model takes the form of $H^{\otimes \lceil \log_2 N \rceil} \otimes R_Z(\theta)$ with Hadamard gates H and a

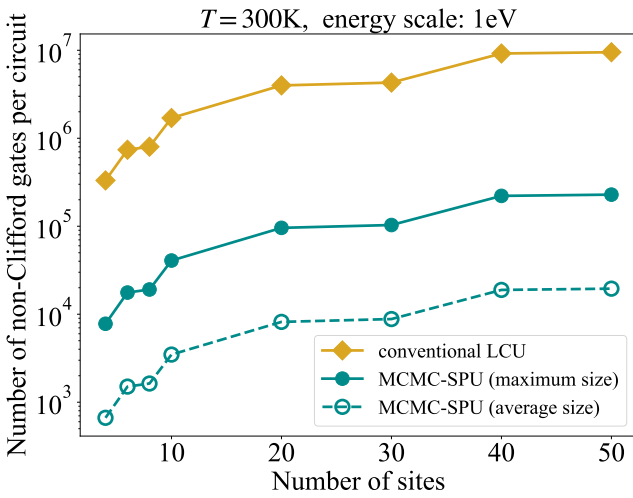
(a)



(b)



(c)



(d)

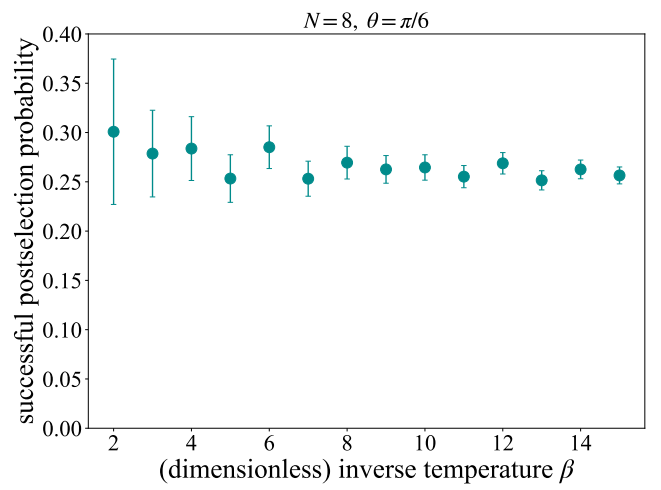


FIG. 5. (a)–(c) Resources required for implementing our MCMC-SPU algorithm and that for the conventional form of the LCU. The Hamiltonian is given by the transverse-field Ising model in Eq. (45). The maximum absolute value of the eigenenergies is set to be 1eV, and the absolute temperature is set to be $T = 300\text{K}$. The truncation order d is determined as $d = 82$ based on Eq. (47) with $\nu = 0.1$. (a) Total number of qubits including ancilla qubits for each quantum circuit. Blue circles (Brown diamonds) represent the total number of qubits required for implementing our MCMC-SPU algorithm (the conventional LCU method as a part of the QMETTS algorithm). (b)–(c) Gate count of each quantum circuit, where we decompose each quantum circuit into a set of Clifford gates and single-qubit non-Clifford rotation gates. (b) Number of Clifford gates appearing in each quantum circuit. Brown diamonds represent the number of Clifford gates required for implementing the conventional LCU method as a part of the QMETTS algorithm. Blue filled (empty) circles represent the maximum number (the average weighted by the sampling probability) of Clifford gates per quantum circuit appearing in stochastically sampling pairs (m, n) of orders in our MCMC-SPU algorithm (see Steps 1.–2. in Sec. III A). (c) Number of non-Clifford single-qubit rotation gates appearing in each quantum circuit. Brown diamonds represent the number of non-Clifford single-qubit rotation gates required for implementing the conventional LCU method as a part of the QMETTS algorithm. Blue filled (empty) circles represent the maximum number (the average weighted by the sampling probability) of those gates per quantum circuit in stochastically sampling pairs (m, n) of orders in our MCMC-SPU algorithm. (d) Successful postselection probability for the quantum circuits in our MCMC-SPU algorithm. The plot shows the unweighted average values with error bars representing the standard errors calculated over all the possible pairs (m, n) of orders satisfying $m \leq d$ and $n \leq d$, where d is given by Eq. (47) for each value of the dimensionless inverse temperature β .

single-qubit rotation gate $R_Z(\theta)$. Furthermore, the operator $2|0\rangle_{A,H}\langle 0| - I_A$ is implemented with a multi-controlled phase gate, and SELECT_H in Eq. (18) takes the form as shown in Fig. 2(b). In implementing multi-controlled unitary gates $C^{N_c}(U)$ for these operators, we employ the usual nesting structure by recursively constructing $C^{N_c-1}(U)$ gate sandwiched between two Toffoli gates [110, 111], and we assume that each Toffoli gate is implemented with three single-qubit rotation gates [111]. Figures 5(a)–(c) show the number of qubits and quantum gates required for implementing each quantum circuit, where the Hamiltonian is given by the transverse-field Ising model in Eq. (45). The results in these figures are independent of the value of θ . The eigenvalues of the Hamiltonian are rescaled so that the maximum absolute value of the eigenenergies is set to be 1eV, and the absolute temperature is set to be $T = 300\text{K}$, from which the truncation order d of the LCU is determined as $d = 82$ based on Eq. (47) with $\nu = 0.1$.

Figure 5(a) shows the total number of qubits including ancilla qubits for each quantum circuit. For both the conventional LCU implementation (brown diamonds) and our MCMC-SPU (blue circles), the total numbers of qubits exhibit nearly linear scaling with the number N of sites, while the latter requires fewer ancilla qubits.

We next discuss the gate count of each quantum circuit. We decompose each quantum circuit into a set of Clifford gates and single-qubit non-Clifford rotation gates. Note that we do not decompose a single-qubit non-Clifford rotation gate into a large number of Clifford gates and T gates on the basis of the assumption that such decomposition is beyond the capability of early-FTQC devices (see Sec. VI for a discussion on direct implementation of single-qubit rotation gates). Figure 5(b) shows the number of Clifford gates appearing in each quantum circuit. The maximum number of Clifford gates per circuit appearing in the stochastic sampling in our MCMC-SPU algorithm (blue filled circles) is about two orders of magnitude smaller than that for the conventional implementation of the LCU (brown diamonds). Furthermore, the average number of Clifford gates per circuit weighted by the sampling probability of each pair of orders in our MCMC-SPU (blue empty circles) is about three orders of magnitude smaller than that for the conventional implementation (brown diamonds).

Figure 5(c) shows the number of non-Clifford single-qubit rotation gates appearing in each quantum circuit. Similar to the case of Clifford gates, the maximum number of non-Clifford single-qubit rotation gates per circuit in the stochastic sampling in our MCMC-SPU (blue filled circles) is about two orders of magnitude smaller than that for the conventional LCU implementation (brown diamonds). Moreover, the average number of those gates per circuit weighted by the sampling probability of each pair of orders in our MCMC-SPU (blue empty circles) is about three orders of magnitude smaller than that for the conventional implementation (brown diamonds).

In summary, our MCMC-SPU algorithm can be im-

plemented with smaller numbers of qubits and quantum gates compared to the conventional implementation of the LCU. In particular, the required number of quantum gates is reduced by orders of magnitude. Even if the absolute temperature is set to be a value different from $T = 300\text{K}$, the required numbers of qubits and quantum gates exhibit similar scaling as a function of the number of sites. Furthermore, our MCMC-SPU exhibits a better scaling for the required implementation resources with increasing β , making it suitable for the early-FTQC era, since the average value d_{average} of a sampled order scales as $\mathcal{O}(\sqrt{\beta})$ in our MCMC-SPU while the conventional implementation of LCU deterministically involves depth of $\mathcal{O}(\sum_{k=0}^d k) = \mathcal{O}(\beta^2)$ and $\mathcal{O}(\log_2 d) = \mathcal{O}(\log_2 \beta)$ ancilla qubits for superposition [see Eq. (47)].

B. Probability of successful postselection

We discuss the probability of the successful postselection on the measurement outcomes of the ancilla qubits with labels A and \bar{A} for each quantum circuit (see Fig. 4 and Step 5. in Sec. III A) appearing in the MCMC-SPU algorithm. We perform a numerical simulation for the one-dimensional transverse-field Ising model in Eq. (45) with $N = 8$ and $\theta = \pi/6$ as an illustrative example. The numerical simulation is performed with the Qulacs package [112]. In Fig. 5(d), we show the numerical results of the successful postselection probability for the quantum circuits in our MCMC-SPU algorithm. The plot shows the unweighted average value calculated over all the possible pairs (m, n) of orders satisfying $m \leq d$ and $n \leq d$ (see Appendix C for the detailed data), where d is given by Eq. (47) for each value of the dimensionless inverse temperature β . The results presented in Fig. 5(d) exhibit almost constant successful postselection probability, avoiding exponential decay with β . This fact stands in stark contrast to an exponential decay with β observed in the conventional LCU implementation (see Sec. II B 2). Note that the lower bound on the successful postselection probability for each quantum circuit in implementing the single-ancilla LCU for a general matrix function is obtained in Ref. [72]. This lower bound for each quantum circuit is independent of the value of β in our implementation since the β dependence appears only in the probability distribution for the stochastic sampling of orders through the coefficients $\{c_n\}$ in Eq. (29). Detailed analysis on the β dependence of the weighted average of the lower bounds over all the possible pairs of orders is left for future work.

C. Number of quantum circuits

We now discuss the number of quantum circuits required for our MCMC-SPU algorithm. Since the quantity in the numerator (denominator) of the right-hand side of

Eq. (36) is given by a statistical mean of a stochastic variable that lies in the range $[-\|O\|_{\text{op}} \cdot \|c\|_1^2, \|O\|_{\text{op}} \cdot \|c\|_1^2]$ ($[-\|c\|_1^2, \|c\|_1^2]$), the Hoeffding's inequality [113] tells us that the required number $N_{\epsilon,\delta}$ of pairs of orders, equivalent to the number of quantum circuits, is given by

$$N_{\epsilon,\delta} = \mathcal{O}\left[\frac{\|c\|_1^4}{\epsilon^2} \log\left(\frac{2}{\delta}\right)\right] = \mathcal{O}\left[\frac{e^{2\beta}}{\epsilon^2} \log\left(\frac{2}{\delta}\right)\right] \quad (50)$$

to ensure that the error of the statistical mean from the true expectation value is bounded by ϵ with probability $1 - \delta$. This analysis only considers the statistical error ϵ , and the sampling overhead involved with calculating the quantum-mechanical expectation value is not taken into account. In Eq. (50), we use Eq. (49) for the d -th-order approximation $\tilde{f}(\cdot)$ of $f(\cdot)$ satisfying Eq. (46) [86] while omitting the scaling of a sufficiently small quantity ν . The scaling of $N_{\epsilon,\delta} \propto e^{2\beta}$ for the number of circuits in our MCMC-SPU algorithm is equivalent to that for the required number N_{PS} of trials until realization of a successful postselection in the conventional LCU implementation (see Eq. (21) and the following argument). This fact, together with the results in Sec. IV B, tells us that the required total number of executions of quantum circuits, which is defined as the product of the number of circuits and the inverse of the successful postselection probability, exhibits a scaling $\mathcal{O}(e^{2\beta})$ similar to the case for the conventional LCU implementation (see also Ref. [86]). Note that we can perform a parallel operation of several kinds of quantum circuits U_{mn} 's on independent quantum devices in our MCMC-SPU algorithm in contrast to the conventional implementation (see also Fig. 1).

V. NUMERICAL DEMONSTRATION OF THE MCMC-SPU ALGORITHM

We present a numerical demonstration of our MCMC-SPU algorithm by applying it to the one-dimensional transverse-field Ising model in Eq. (45) with $N = 6$ and $\theta = \pi/8$ as an illustrative example. The maximum absolute value of the eigenenergies is set to be 0.1eV. The truncation order d is determined by Eq. (47) with $\nu = 0.002$, and our numerical demonstration does not involve simulated noise. For a practical calculation, as is usually done for Markov-chain Monte-Carlo simulations in general [89–92], we first evaluate the initial-relaxation time step n_{relax} , during which the dependence on a randomly chosen initial state gradually vanishes. To suppress the influence of the randomly chosen initial state, we then consider the statistical ensemble consisting of samples after the initial relaxation. To appropriately evaluate the number n_{eff} of effectively independent samples, we examine the autocorrelation time step τ after the initial relaxation. Specifically, it is evaluated as the number of samples n_{sample} belonging to the statistical ensemble divided by twice the integrated autocorrelation

time step τ , i.e., $n_{\text{eff}} = n_{\text{sample}}/(2\tau)$. Finally, we demonstrate that our MCMC-SPU algorithm provides the correct finite-temperature value of an observable. In the following subsections, we discuss each step of the above procedure.

A. Initial relaxation

We first consider an initial-relaxation time step n_{relax} , during which the dependence on the randomly chosen initial state gradually vanishes. The first n_{relax} steps are called the burn-in period, and the samples belonging to this period are excluded from the statistical ensemble.

In our analysis, for each quantum circuit appearing in our MCMC-SPU algorithm (see Fig. 4), we focus on two qualitatively different initial states, $|\psi_F\rangle = |000000\rangle$ and $|\psi_{\text{AF}}\rangle = |010101\rangle$, and generate a series of measurement outcomes of an observable generated in the MCMC sampling for each of these two initial states. We estimate the initial-relaxation time step as the time step at which the two series of results generated by the two initial states $|\psi\rangle$ and $|\psi_{\text{AF}}\rangle$ become statistically indistinguishable (see Appendix D for technical details of the analysis on the initial relaxation).

In Fig. 6, we show the numerical results of the initial-relaxation time step for each quantum circuit U_{mn} appearing in the MCMC-SPU algorithm for the transverse-field Ising model. Figure 6(a) [(b)] shows the initial-relaxation time step evaluated conditioned on the measurement outcome of the ancilla qubit for superposition with label \bar{A} being zero [one] for the quantum circuit U_{mn} , which involves unitary gates U_m and U_n corresponding to a pair of orders m and n stochastically sampled from the expansion of an imaginary-time evolution (see Steps 1–2. in Sec. III A). For most pairs of orders shown in Fig. 6, which are relevant in the following numerical simulation, the resulting values of the initial-relaxation time step are less than 40 (see Appendix B for the system-size dependence). These results are of the same order as that for the conventional LCU implementation (see Sec. II B 1), which is obtained as 10 by our numerical evaluation.

B. Autocorrelation

We consider the autocorrelation time step after the initial relaxation for each quantum circuit appearing in our MCMC-SPU algorithm. An autocorrelation time step is defined as the number of successive samples in the MCMC sampling among which a statistical correlation cannot be neglected. The effective number n_{eff} of independent samples is determined by dividing the number n_{sample} of all the samples belonging to the statistical ensemble by twice the integrated autocorrelation time step τ , i.e., $n_{\text{eff}} = n_{\text{sample}}/(2\tau)$. We employ the jackknife method [114–117] to numerically determine the autocor-

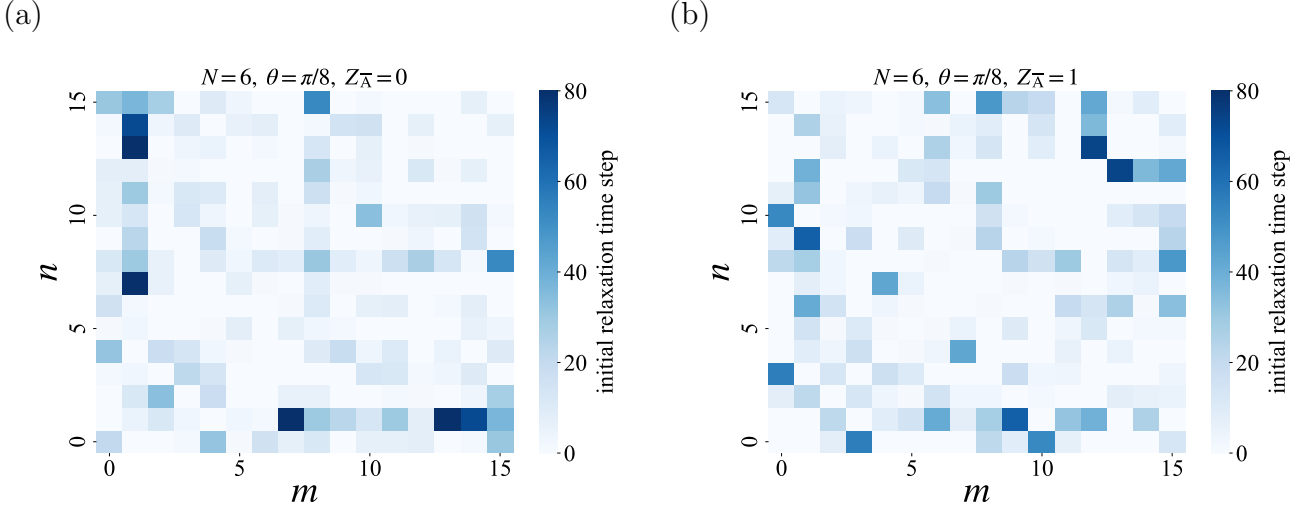


FIG. 6. Initial-relaxation time step for each quantum circuit appearing in the MCMC-SPU algorithm for the one-dimensional transverse-field Ising model with six sites. The plots show the initial-relaxation time step evaluated conditioned on the measurement outcome of the ancilla qubit for superposition with label \bar{A} being (a) $Z_{\bar{A}} = 0$ and (b) $Z_{\bar{A}} = 1$ for the quantum circuit U_{mn} . This quantum circuit involves unitary gates U_m and U_n corresponding to a pair of orders m and n stochastically sampled from the expansion of an imaginary-time evolution. In Fig. (b), although the results are plotted as zero for $m = n$ for convenience, they actually intend to represent that we do not perform an MCMC sampling for these combinations of indices (see Eq. (35) and the following argument).

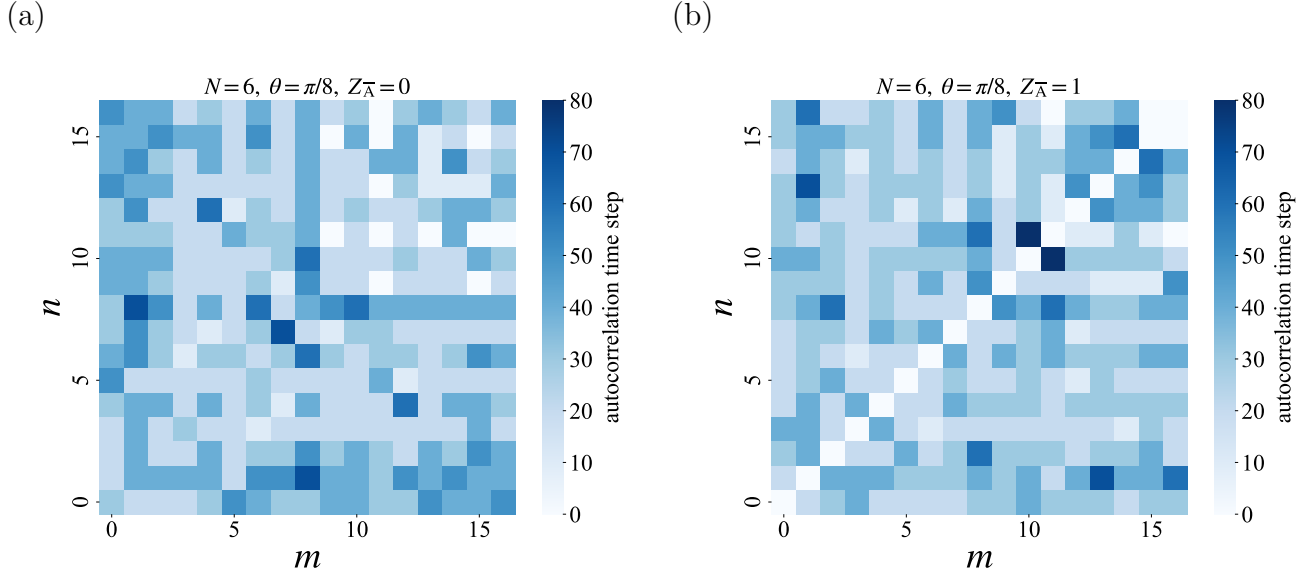


FIG. 7. Autocorrelation time step for each quantum circuit appearing in the MCMC-SPU algorithm for the one-dimensional transverse-field Ising model with six sites. The plots show the autocorrelation time step evaluated conditioned on the measurement outcome of the ancilla qubit for superposition with label \bar{A} being (a) $Z_{\bar{A}} = 0$ and (b) $Z_{\bar{A}} = 1$ for the quantum circuit U_{mn} . This quantum circuit involves unitary gates U_m and U_n corresponding to a pair of orders m and n stochastically sampled from the expansion of an imaginary-time evolution. In Fig. (b), although the results are plotted as zero for $m = n$ for convenience, they actually intend to represent that we do not perform an MCMC sampling for these combinations of indices (see Eq. (35) and the following argument).

relation time step (see Appendix E for details of the jackknife method).

Figure 7 shows the numerical results of the autocorrelation time step for each quantum circuit U_{mn} (see Fig. 4) in our MCMC-SPU. Figure 7(a) [(b)] shows the results

evaluated under the condition that the measurement outcome of the ancilla qubit for superposition with label \bar{A} is $Z_{\bar{A}} = 0$ [$Z_{\bar{A}} = 1$] for the quantum circuit U_{mn} . For most pairs of orders shown in Fig. 7, the numerical results are less than 60 (see Appendix B for the system-size depen-

dence). These results are of the same order as that for the conventional LCU implementation (see Sec. II B 1), which is obtained as 10 by our numerical evaluation. These results, together with those in Sec. V A, indicate that the statistical sampling overhead for the MCMC-SPU algorithm for each quantum circuit is not considerably large compared with that for the QMETTS with the conventional LCU implementation.

C. Thermal average of an observable

On the basis of the analysis in the previous subsections, we calculate the thermal-equilibrium expectation value of an observable at finite temperature using our MCMC-SPU algorithm. Figure 8 shows the thermal expectation value of the energy calculated with our MCMC-SPU algorithm (blue circles) and with the QMETTS with the conventional LCU implementation (brown diamonds), the error bars include the statistical error and the error from the exact canonical-ensemble average (gray dashed curve) due to the truncation of the polynomial expansion of an imaginary-time evolution [see Eq. (24)]. The statistical error for the MCMC-SPU is calculated on the

basis of the standard errors for each of the numerator and the denominator on the right-hand side of Eq. (37). The contribution of the truncation error is included only below the plotted points. The results of both algorithms agree well with the exact canonical-ensemble average (gray dashed curve) within the error bars. The uniform shift in the plots from the exact value originates from the truncation error [see Eq. (24)].

VI. DISCUSSION AND CONCLUSION

In this paper, we have proposed the MCMC-SPU algorithm, which is a method to calculate the thermal-equilibrium expectation value of an observable at finite temperature. Our proposal is well-suited for implementation on early-FTQC devices. Our proposal is implemented with a set of simple quantum circuits, each of which involves a pair of unitary gates U_m and U_n (see Fig. 4) stochastically sampled from the set of the unitary gates $\{U_0, U_1, \dots, U_d\}$ appearing in the conventional LCU method (see Fig. 2). For each quantum circuit consisting of the two unitary gates, a statistical ensemble unique to the circuit is generated as a stationary distribution of the MCMC sampling as a part of the algorithm.

We have discussed that stochastic sampling of orders in the MCMC-SPU algorithm leads to a significant reduction in the implementation resources such as qubits and quantum gates compared with the conventional implementation of the LCU. The required number of quantum gates is reduced by orders of magnitude (see Sec. IV A), making our MCMC-SPU algorithm well-suited for the early-FTQC era (see the discussion below about the possibility of implementation on a prototypical device). We have also discussed that the required total number of quantum-circuit executions, which is defined as the product of the number of circuits and the inverse of the successful postselection probability, for the MCMC-SPU algorithm exhibits a scaling $\mathcal{O}(e^{2\beta})$ similar to the case for the conventional LCU implementation (see Secs. IV B and IV C).

To demonstrate the validity of our proposal, we have performed a numerical simulation of our MCMC-SPU algorithm by applying it to the one-dimensional transverse-field Ising model as an illustrative example. We have discussed that the statistical sampling overhead, which is accompanied by the initial relaxation and the autocorrelation, for the MCMC-SPU algorithm for each quantum circuit is not considerably large compared with that for the QMETTS with the conventional LCU implementation (see Secs. V A and V B). We have calculated the thermal-equilibrium expectation value of the energy at finite temperature and found that the results of the MCMC-SPU algorithm agree well with the exact results within the statistical error and the truncation error (see Sec. V C).

We now discuss the possibility of implementing our MCMC-SPU algorithm on a prototypical example of

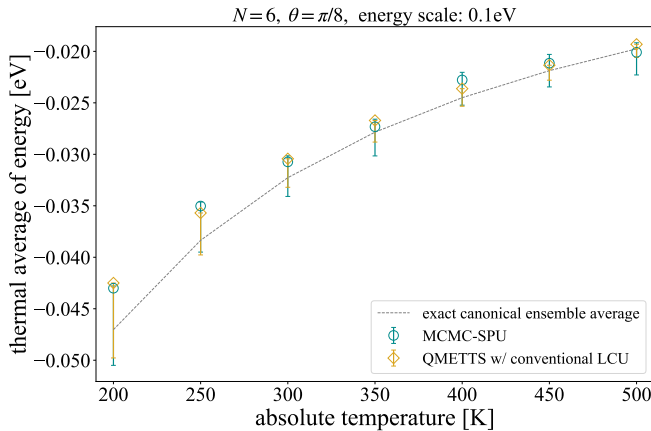


FIG. 8. The thermal-equilibrium expectation value of the energy calculated with our MCMC-SPU algorithm (blue circles) and with the QMETTS with the conventional LCU implementation (brown diamonds). The error bars include the statistical error and the truncation error [see Eq. (24)] from the exact canonical-ensemble average (gray dashed curve). The statistical error is calculated on the basis of the standard errors for each of the numerator and the denominator on the right-hand side of Eq. (37). The contribution of the truncation error is included only below the plotted points. The Hamiltonian is given by the one-dimensional transverse-field Ising model with parameters $N = 6$ and $\theta = \pi/8$ [see Eq. (45)], where the maximum absolute value of the eigenenergies is set to be 0.1eV. In the numerical simulation, ϵ in Eq. (50) is set to be $\epsilon = 0.1$. In the calculation with the MCMC-SPU (QMETTS) algorithm, the burn-in period and the autocorrelation time step are set to be 100 (10) on the basis of the results in Secs. V A and V B.

early-FTQC devices. As a specific example, we consider the Space-Time efficient Analog Rotation quantum computing architecture (STAR architecture), which was recently proposed in Ref. [83]. This architecture can realize the universal quantum computation with the combination of fault-tolerant Clifford gates and non-fault-tolerant analog rotation gates without the T-gate decomposition. An analog rotation gate is implemented using the gate teleportation with the corresponding magic state. Analog rotation gates are not fault-tolerant and are therefore the major source of logical errors in the STAR architecture. The corresponding logical error rate P_{rotation} is obtained as $P_{\text{rotation}} = 2p_{\text{phys}}/15 + \mathcal{O}(p_{\text{phys}}^2)$ with the physical error rate p_{phys} [83]. This logical error can be suppressed by performing the probabilistic error cancellation with a reasonable sampling overhead if the number N_{rotation} of analog rotation gates satisfies $N_{\text{rotation}} P_{\text{rotation}} \leq 2$ [118]. This condition can be rewritten as $p_{\text{phys}} \leq 15N_{\text{rotation}}^{-1}$. Combining this condition with the results in Fig. 5(c), we discuss the physical error rate required to implement our MCMC-SPU and the QMETTS algorithm with the conventional implementation of the LCU. We focus on models with about fifty sites, which can be hardly simulated on classical computers. The physical error rate required to implement the conventional form of the LCU is $p_{\text{phys}} \simeq 10^{-6}$, which is currently difficult to achieve with existing technology. In contrast, the physical error rate required to implement a quantum circuit with the maximum [average] size in our MCMC-SPU algorithm is $p_{\text{phys}} \simeq \mathcal{O}(10^{-4})$ [$p_{\text{phys}} \simeq \mathcal{O}(10^{-3})$]. In particular, the required physical error rate for the average-sized circuit is within the scope of the current technology, depending on the choice of hardware [119–123]. Note that even for more complicated models of practical interest, such as fermionic systems, gate counts and the required physical error rate are expected to exhibit a similar scaling under general assumptions such as the spatial translational invariance and the locality of the interactions.

We here discuss some remarks on our method compared with other possible techniques for simulating thermal-equilibrium systems at finite temperature. First, it is known that the amplitude-amplification technique [73–76, 104–107, 124] can be inserted before performing measurement and postselection on the ancilla qubits for the conventional form of the LCU method, leading to enhancing the successful postselection probability [86, 107]. A similar technique could also be applied to the MCMC-SPU algorithm although the MCMC-SPU does not significantly suffer from a decay in the postselection probability (see Sec. IV B and Appendix C). Despite the potential usefulness of such a technique in amplifying the successful postselection probability with respect to the measurement outcomes on the ancilla qubits, inserting this step leads to an increase in circuit depth. Second, while we employ a method that involves generating statistical ensembles to simulate finite-temperature systems,

as done in the METTS algorithm, we could alternatively employ a method based on pure states such as the technique of the thermal pure quantum (TPQ) states [40–45]. Although such a technique is free from explicitly generating the thermal statistical ensemble, generating a TPQ state involves overhead in preparing a Haar-random state or the unitary t -design [48, 49] as an initial state. The possibilities raised above are beyond the scope of this paper and are left for interesting future problems.

One possible application of our technique is to simulate various physical quantities in more complicated quantum many-body systems, such as electronic conductivity, magnetic susceptibility, and the Green's functions in strongly correlated electron systems. This could potentially contribute to the study on real materials, and we leave such problems for interesting future work. We hope that this work stimulates further investigation into quantum algorithms that exhibit an advantage in simulating the nature of large-scale quantum many-body systems.

ACKNOWLEDGEMENT

The authors are grateful to Riki Toshio and Yu-taro Akahoshi for helpful comments and discussions. N.M. acknowledges Masatoshi Ishii for technical support in performing numerical simulations.

Appendix A: Efficiency of sampling the weight factor

In this appendix, we present a discussion on the efficiency of sampling the quantity W_{mn}^{ik} , which plays a role in evaluating the numerator and the denominator on the right-hand side of Eq. (37) (see also Eqs. (39) and (40) and the following discussion in Sec. III B). The quantity $2^{-N} Z_{mn}^k = 2^{-N} \sum_{i=0}^{2^N-1} W_{mn}^{ik}$, which appears in both the numerator and the denominator on the right-hand side of Eq. (37), can be obtained as a statistical mean of $\{W_{mn}^{ik}\}$ evaluated by uniform sampling with respect to the label i . The efficiency of this uniform sampling depends on whether the set of values of $\{W_{mn}^{ik}\}$ for a fixed combination of (m, n, k) is close to a uniform distribution. In Fig. 9, we show the standard deviation of the set of values of the quantity W_{mn}^{ik} as a benchmark of the uniformness of the distribution for some representative combinations of parameters (m, n, k) , where the model and the conditions are set to be the same as those in Sec. V. In this figure, the blue circles [brown diamonds] represent the results for the set of values sampled uniformly with respect to the index i while (m, n, k) is fixed to be $(2, 8, 1)$ [$(1, 9, 0)$]. These results indicate that the standard deviation does not exhibit a significant increase with increasing the system size, implying that the distribution of W_{mn}^{ik} does not significantly deviate from a uniform one, at least within the range of our simulation. This result supports the efficiency of our strategy to evaluate Z_{mn}^k by sampling

the label i uniformly.

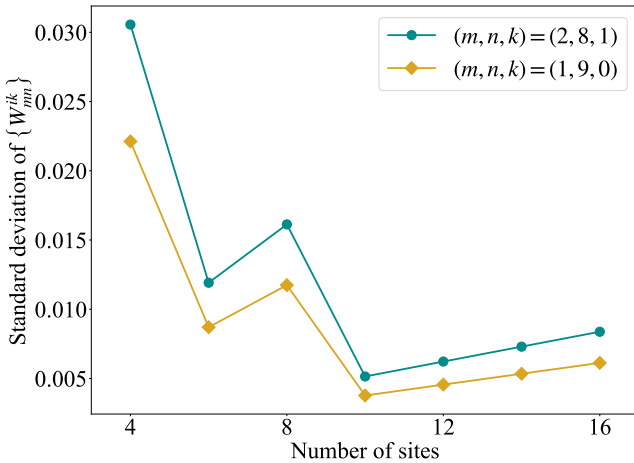


FIG. 9. System-size dependence of the standard deviation of the set of values of the quantity W_{mn}^{ik} . The blue circles [brown diamonds] represent the results for the set of values sampled uniformly with respect to the index i while (m, n, k) is fixed to be $(2, 8, 1)$ [$(1, 9, 0)$].

Appendix B: System-size dependence of the statistical sampling overhead

In this appendix, we discuss the system-size dependence of the initial-relaxation time steps and the autocorrelation time steps (see Secs. V A and V B for the definitions of these quantities). In Fig. 10, we show numerical results for some representative combinations of the values of (m, n, k) , where the model and the conditions are set to be the same as those in Sec. V except for the system size. In this figure, the blue empty [filled] circles represent the initial-relaxation time steps for $(m, n, k) = (1, 9, 1)$ [$(m, n, k) = (1, 7, 0)$], while the brown empty [filled] diamonds represent the autocorrelation time steps for $(m, n, k) = (10, 11, 1)$ [$(m, n, k) = (1, 8, 0)$]. These results indicate that both the initial-relaxation and the autocorrelation time steps do not exhibit an exponential scaling with the system size, which implies the scalability of our MCMC-SPU algorithm, at least within the range of our simulation.

Appendix C: Detailed data of the successful postselection probability

We present the detailed data of the successful postselection probability for each quantum circuit appearing in the MCMC-SPU algorithm, which is discussed in Sec. IV B. We perform a numerical simulation for the one-dimensional transverse-field Ising model in Eq. (45) with

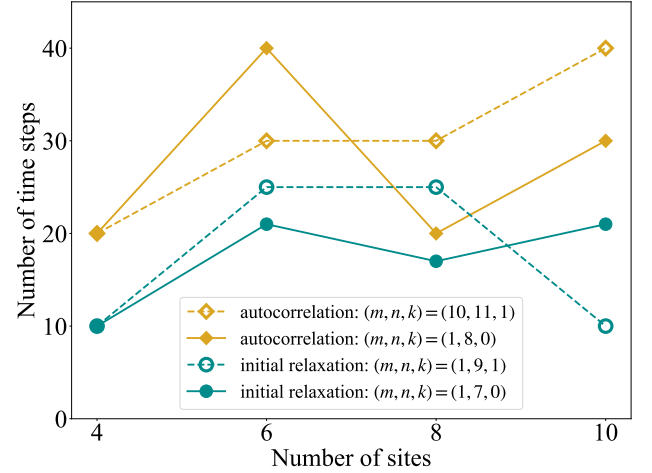


FIG. 10. System-size dependence of the initial-relaxation time steps and the autocorrelation time steps. The blue empty [filled] circles represent the initial-relaxation time steps for $(m, n, k) = (1, 9, 1)$ [$(m, n, k) = (1, 7, 0)$]. The brown empty [filled] diamonds represent the autocorrelation time steps for $(m, n, k) = (10, 11, 1)$ [$(m, n, k) = (1, 8, 0)$].

$N = 8$ and $\theta = \pi/6$ as an illustrative example. In Fig. 11, we show the numerical results of the successful postselection probability for each quantum circuit U_{mn} appearing in the MCMC-SPU algorithm for the transverse-field Ising model. Figure 11(a) [(b)] shows the probability of successful postselection of measurement outcomes on the ancilla qubits, which is evaluated conditioned on the measurement outcome of the ancilla qubit for superposition with index \bar{A} being $Z_{\bar{A}} = 0$ [$Z_{\bar{A}} = 1$] for the quantum circuit U_{mn} . This quantum circuit involves unitary gates U_m and U_n corresponding to a pair of orders m and n stochastically sampled from the expansion of an imaginary-time evolution (see Steps 1.–2. in Sec. III A). These plots show that an appropriate postselection corresponding to each combination of indices $(m, n, Z_{\bar{A}})$ is achieved with nonzero probability except for the case of $(m, m, 1)$ (see Eq. (35) and the following argument). The unweighted average of the results shown in these plots yields the results in Fig. 5(d) in Sec. IV B.

Appendix D: Analysis of the initial relaxation

In this appendix, we present a technical detail of the analysis of the initial-relaxation time step of our MCMC-SPU algorithm in Sec. V A. Our analysis is based on the Gelman-Rubin statistics [125–127], on which we present a brief review in the following. In a general setup, we consider a set of data series $\{\theta_{ij}\}_{ij}$, where θ_{ij} denotes the i -th element of the series labeled with j . In our specific analysis in Sec. V A, the number of series is two and the label $j = 1$ ($j = 2$) corresponds to the initial state $|\psi_F\rangle$

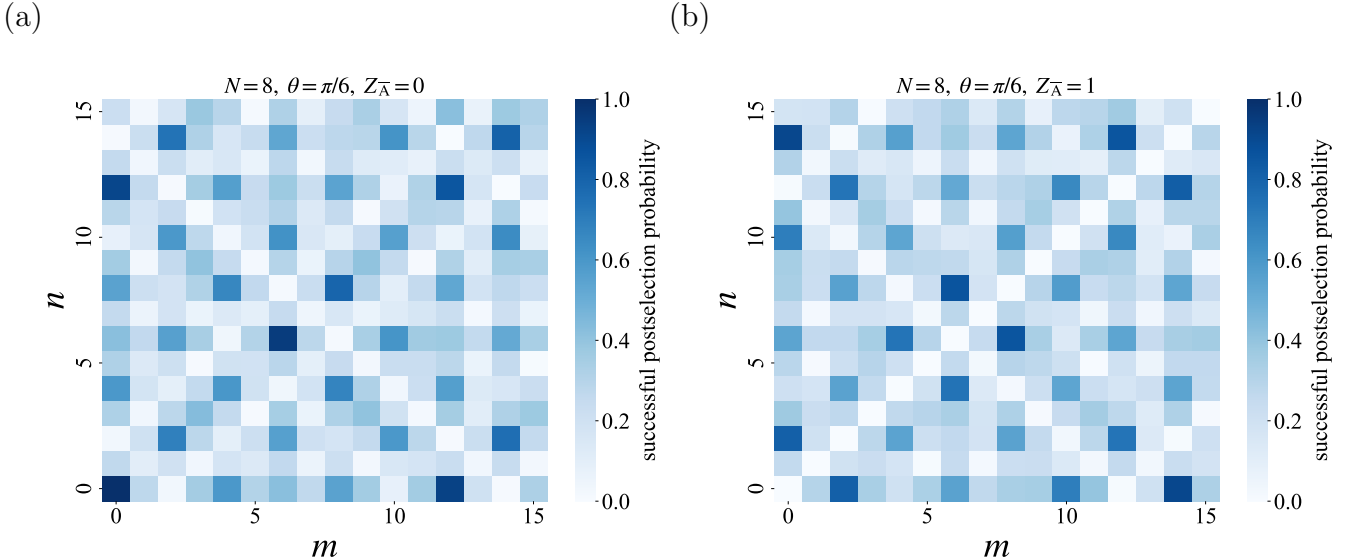


FIG. 11. Successful postselection probability for each quantum circuit appearing in the MCMC-SPU algorithm for the one-dimensional transverse-field Ising model with eight sites. The plots show the probability of successful postselection of measurement outcomes on the ancilla qubits conditioned on the measurement outcome of the ancilla qubit for superposition with index \bar{A} being (a) $Z_{\bar{A}} = 0$ and (b) $Z_{\bar{A}} = 1$, respectively, for the quantum circuit U_{mn} . This quantum circuit involves unitary gates U_m and U_n corresponding to a pair of orders m and n stochastically sampled from the expansion of an imaginary-time evolution. In Fig. (b), although the results for $m = n$ are plotted as zero for convenience, they actually intend to represent that we do not perform an MCMC sampling for these combinations of indices (see Eq. (35) and the following argument).

$(|\psi_{\text{AF}}\rangle)$ for the series of states generated by the Markov process, while the label i represents the time step in each series. We generate $2N_{\text{step}}$ time steps and discard the first N_{step} steps as the burn-in period. We then consider the statistical ensemble consisting of the results of the last N_{step} steps in the following.

We first define the within-chain variance as

$$W_{\text{GR}} := \frac{1}{N_{\text{step}}(N_{\text{series}} - 1)} \sum_{j=1}^{N_{\text{series}}} \sum_{i=1}^{N_{\text{step}}} (\theta_{ij} - \bar{\theta}_j)^2, \quad (\text{D1})$$

where $\bar{\theta}_j$ denotes the mean value of the series $\{\theta_{ij}\}_i$, i.e.,

$$\bar{\theta}_j := \frac{1}{N_{\text{step}}} \sum_{i=1}^{N_{\text{step}}} \theta_{ij}. \quad (\text{D2})$$

We also define the between-chain variance as

$$B_{\text{GR}} := \frac{N_{\text{step}}}{N_{\text{series}} - 1} \sum_{j=1}^{N_{\text{series}}} (\bar{\theta}_j - \bar{\theta})^2, \quad (\text{D3})$$

where $\bar{\theta}$ denotes the mean value of all data appearing in the N_{series} series, i.e.,

$$\bar{\theta} := \frac{1}{N_{\text{step}}N_{\text{series}}} \sum_{j=1}^{N_{\text{series}}} \sum_{i=1}^{N_{\text{step}}} \theta_{ij} = \frac{1}{N_{\text{series}}} \sum_{j=1}^{N_{\text{series}}} \bar{\theta}_j. \quad (\text{D4})$$

On the basis of the two kinds of variance defined in Eqs. (D1) and (D3), we calculate the estimator \hat{V}_{GR} of

the variance of the stationary distribution consisting of the whole data from all the series as follows:

$$\hat{V}_{\text{GR}}(N_{\text{step}}) = \frac{N_{\text{step}} - 1}{N_{\text{step}}} W_{\text{GR}} + \frac{1}{N_{\text{step}}} B_{\text{GR}}. \quad (\text{D5})$$

We then define the potential scale reduction factor $\hat{R}_{\text{GR}}(N_{\text{step}})$ as

$$\hat{R}_{\text{GR}}(N_{\text{step}}) := \sqrt{\frac{\hat{V}_{\text{GR}}(N_{\text{step}})}{W_{\text{GR}}}}. \quad (\text{D6})$$

If this quantity takes a value such that $\hat{R}_{\text{GR}}(N_{\text{step}}) \leq 1.1$, we conclude that N_{series} series are statistically indistinguishable and that the convergence has been achieved [126, 127]. In our specific analysis in Sec. V A, we conclude that N_{step} is sufficient as the burn-in period if the above condition is satisfied.

Appendix E: Jackknife method and autocorrelation

In this appendix, we present a brief review of the general theory of the jackknife method [114–117], which is employed in the analysis of the autocorrelation time step in our MCMC-SPU algorithm in Sec. V B. The autocorrelation in a sequence of data can be evaluated using the jackknife method with bin size s_{bin} . We first divide the series $\{A_l\}_l$ of M_{data} data into $M_b = M_{\text{data}}/s_{\text{bin}}$ bins,

and then define $\langle A \rangle_b$ for each label b of bin as

$$\langle A \rangle_b := \frac{1}{M_{\text{data}} - s_{\text{bin}}} \sum_{l \notin B_b} A_l, \quad (\text{E1})$$

where B_b denotes the bin of data with label b . Then we obtain the mean of the function $f(A)$ of the data A as

$$\langle f(A) \rangle = \frac{1}{M_b} \sum_{b=1}^{M_b} f(\langle A \rangle_b) \quad (\text{E2})$$

with its standard error

$$\delta \langle f(A) \rangle = \sqrt{(M_b - 1) [\langle f(A)^2 \rangle - \langle f(A) \rangle^2]}. \quad (\text{E3})$$

If the bin size s_{bin} is sufficiently large compared with the autocorrelation time step τ , bins with different labels are effectively regarded as uncorrelated with one another and the standard error $\delta \langle f(A) \rangle$ is independent of the bin size s_{bin} . On the basis of this observation, we gradually increase the bin size s_{bin} and examine the spin-dependence of the standard error $\delta \langle f(A) \rangle$. If the value of $\delta \langle f(A) \rangle$ saturates and becomes stationary within fluctuations when the bin size is set to be $s_{\text{bin}} = 2\tau$, the integrated autocorrelation time step is estimated as τ . In our specific analysis in Sec. V B, the data A corresponds to the label of the state of the target system in the computational basis, and the function $f(A)$ corresponds to the value of an observable.

[1] A. Ekert and R. Jozsa, Quantum computation and shor's factoring algorithm, *Rev. Mod. Phys.* **68**, 733 (1996).

[2] A. Steane, Quantum computing, *Reports on Progress in Physics* **61**, 117 (1998).

[3] T. D. Ladd, F. Jelezko, R. Laflamme, Y. Nakamura, C. Monroe, and J. L. O'Brien, Quantum computers, *Nature* **464**, 45 (2010).

[4] Y. Cao, J. Romero, J. P. Olson, M. Degroote, P. D. Johnson, M. Kieferová, I. D. Kivlichan, T. Menke, B. Peropadre, N. P. Sawaya, *et al.*, Quantum chemistry in the age of quantum computing, *Chemical reviews* **119**, 10856 (2019).

[5] L. Gyongyosi and S. Imre, A survey on quantum computing technology, *Computer Science Review* **31**, 51 (2019).

[6] R. Orús, S. Mugel, and E. Lizaso, Quantum computing for finance: Overview and prospects, *Reviews in Physics* **4**, 100028 (2019).

[7] C. Outeiral, M. Strahm, J. Shi, G. M. Morris, S. C. Benjamin, and C. M. Deane, The prospects of quantum computing in computational molecular biology, *WIREs Computational Molecular Science* **11**, e1481 (2021).

[8] S. S. Gill, A. Kumar, H. Singh, M. Singh, K. Kaur, M. Usman, and R. Buyya, Quantum computing: A taxonomy, systematic review and future directions, *Software: Practice and Experience* **52**, 66 (2022).

[9] M. Lewenstein, A. Sanpera, V. Ahufinger, B. Damski, A. Sen(De), and U. Sen, Ultracold atomic gases in optical lattices: mimicking condensed matter physics and beyond, *Advances in Physics* **56**, 243 (2007).

[10] I. Buluta and F. Nori, Quantum simulators, *Science* **326**, 108 (2009).

[11] I. Kassal, J. D. Whitfield, A. Perdomo-Ortiz, M.-H. Yung, and A. Aspuru-Guzik, Simulating chemistry using quantum computers, *Annual Review of Physical Chemistry* **62**, 185 (2011).

[12] I. M. Georgescu, S. Ashhab, and F. Nori, Quantum simulation, *Rev. Mod. Phys.* **86**, 153 (2014).

[13] P. J. J. O'Malley, R. Babbush, I. D. Kivlichan, J. Romero, J. R. McClean, R. Barends, J. Kelly, P. Roushan, A. Tranter, N. Ding, B. Campbell, Y. Chen, Z. Chen, B. Chiaro, A. Dunsworth, A. G. Fowler, E. Jeffrey, E. Lucero, A. Megrant, J. Y. Mutus, M. Neeley, C. Neill, C. Quintana, D. Sank, A. Vainsencher, J. Wenner, T. C. White, P. V. Coveney, P. J. Love, H. Neven, A. Aspuru-Guzik, and J. M. Martinis, Scalable quantum simulation of molecular energies, *Phys. Rev. X* **6**, 031007 (2016).

[14] E. Zohar, J. I. Cirac, and B. Reznik, Quantum simulations of lattice gauge theories using ultracold atoms in optical lattices, *Reports on Progress in Physics* **79**, 014401 (2015).

[15] C. Noh and D. G. Angelakis, Quantum simulations and many-body physics with light, *Reports on Progress in Physics* **80**, 016401 (2016).

[16] C. Hempel, C. Maier, J. Romero, J. McClean, T. Monz, H. Shen, P. Jurcevic, B. P. Lanyon, P. Love, R. Babbush, A. Aspuru-Guzik, R. Blatt, and C. F. Roos, Quantum chemistry calculations on a trapped-ion quantum simulator, *Phys. Rev. X* **8**, 031022 (2018).

[17] C. Kokail, C. Maier, R. van Bijnen, T. Brydges, M. K. Joshi, P. Jurcevic, C. A. Muschik, P. Silvi, R. Blatt, C. F. Roos, *et al.*, Self-verifying variational quantum simulation of lattice models, *Nature* **569**, 355 (2019).

[18] B. Bauer, S. Bravyi, M. Motta, and G. K.-L. Chan, Quantum algorithms for quantum chemistry and quantum materials science, *Chemical Reviews* **120**, 12685 (2020).

[19] C. W. Bauer, Z. Davoudi, A. B. Balantekin, T. Bhattacharya, M. Carena, W. A. de Jong, P. Draper, A. El-Khadra, N. Gemelke, M. Hanada, D. Kharzeev, H. Lamm, Y.-Y. Li, J. Liu, M. Lukin, Y. Meurice, C. Monroe, B. Nachman, G. Pagano, J. Preskill, E. Rinaldi, A. Roggero, D. I. Santiago, M. J. Savage, I. Siddiqi, G. Siopsis, D. Van Zanten, N. Wiebe, Y. Yamauchi, K. Yeter-Aydeniz, and S. Zorzetti, Quantum simulation for high-energy physics, *PRX Quantum* **4**, 027001 (2023).

(2023).

[20] R. Gerritsma, G. Kirchmair, F. Zähringer, E. Solano, R. Blatt, and C. Roos, Quantum simulation of the dirac equation, *Nature* **463**, 68 (2010).

[21] A. Peruzzo, J. McClean, P. Shadbolt, M.-H. Yung, X.-Q. Zhou, P. J. Love, A. Aspuru-Guzik, and J. L. O'brien, A variational eigenvalue solver on a photonic quantum processor, *Nature communications* **5**, 4213 (2014).

[22] J. R. McClean, J. Romero, R. Babbush, and A. Aspuru-Guzik, The theory of variational hybrid quantum-classical algorithms, *New Journal of Physics* **18**, 023023 (2016).

[23] A. Kandala, A. Mezzacapo, K. Temme, M. Takita, M. Brink, J. M. Chow, and J. M. Gambetta, Hardware-efficient variational quantum eigensolver for small molecules and quantum magnets, *Nature* **549**, 242 (2017).

[24] N. Moll, P. Barkoutsos, L. S. Bishop, J. M. Chow, A. Cross, D. J. Egger, S. Filipp, A. Fuhrer, J. M. Gambetta, M. Ganzhorn, A. Kandala, A. Mezzacapo, P. Müller, W. Riess, G. Salis, J. Smolin, I. Tavernelli, and K. Temme, Quantum optimization using variational algorithms on near-term quantum devices, *Quantum Science and Technology* **3**, 030503 (2018).

[25] J. Preskill, Quantum computing in the nisq era and beyond, *Quantum* **2**, 79 (2018).

[26] M. Cerezo, A. Arrasmith, R. Babbush, S. C. Benjamin, S. Endo, K. Fujii, J. R. McClean, K. Mitarai, X. Yuan, L. Cincio, *et al.*, Variational quantum algorithms, *Nature Reviews Physics* **3**, 625 (2021).

[27] K. Bharti, A. Cervera-Lierta, T. H. Kyaw, T. Haug, S. Alperin-Lea, A. Anand, M. Degroote, H. Heimonen, J. S. Kottmann, T. Menke, W.-K. Mok, S. Sim, L.-C. Kwek, and A. Aspuru-Guzik, Noisy intermediate-scale quantum algorithms, *Rev. Mod. Phys.* **94**, 015004 (2022).

[28] A. Y. Kitaev, Quantum measurements and the abelian stabilizer problem (1995), [arXiv:quant-ph/9511026 \[quant-ph\]](https://arxiv.org/abs/quant-ph/9511026).

[29] R. Cleve, A. Ekert, C. Macchiavello, and M. Mosca, Quantum algorithms revisited, *Proceedings of the Royal Society of London. Series A: Mathematical, Physical and Engineering Sciences* **454**, 339 (1998).

[30] D. S. Abrams and S. Lloyd, Quantum algorithm providing exponential speed increase for finding eigenvalues and eigenvectors, *Phys. Rev. Lett.* **83**, 5162 (1999).

[31] B. L. Higgins, D. W. Berry, S. D. Bartlett, H. M. Wiseman, and G. J. Pryde, Entanglement-free heisenberg-limited phase estimation, *Nature* **450**, 393 (2007).

[32] U. Dorner, R. Demkowicz-Dobrzanski, B. J. Smith, J. S. Lundeen, W. Wasilewski, K. Banaszek, and I. A. Walmsley, Optimal quantum phase estimation, *Phys. Rev. Lett.* **102**, 040403 (2009).

[33] D. Ceperley and B. Alder, Quantum monte carlo, *Science* **231**, 555 (1986).

[34] A. W. Sandvik and J. Kurkijärvi, Quantum monte carlo simulation method for spin systems, *Phys. Rev. B* **43**, 5950 (1991).

[35] W. M. C. Foulkes, L. Mitas, R. J. Needs, and G. Rajagopal, Quantum monte carlo simulations of solids, *Rev. Mod. Phys.* **73**, 33 (2001).

[36] B. M. Austin, D. Y. Zubarev, and W. A. Lester Jr., Quantum monte carlo and related approaches, *Chemical Reviews* **112**, 263 (2012).

[37] J. Carlson, S. Gandolfi, F. Pederiva, S. C. Pieper, R. Schiavilla, K. E. Schmidt, and R. B. Wiringa, Quantum monte carlo methods for nuclear physics, *Rev. Mod. Phys.* **87**, 1067 (2015).

[38] S. R. White, Minimally entangled typical quantum states at finite temperature, *Phys. Rev. Lett.* **102**, 190601 (2009).

[39] E. M. Stoudenmire and S. R. White, Minimally entangled typical thermal state algorithms, *New Journal of Physics* **12**, 055026 (2010).

[40] S. Sugiura and A. Shimizu, Thermal pure quantum states at finite temperature, *Phys. Rev. Lett.* **108**, 240401 (2012).

[41] S. Sugiura and A. Shimizu, Canonical thermal pure quantum state, *Phys. Rev. Lett.* **111**, 010401 (2013).

[42] M. Hyuga, S. Sugiura, K. Sakai, and A. Shimizu, Thermal pure quantum states of many-particle systems, *Phys. Rev. B* **90**, 121110 (2014).

[43] H. Endo, C. Hotta, and A. Shimizu, From linear to non-linear responses of thermal pure quantum states, *Phys. Rev. Lett.* **121**, 220601 (2018).

[44] A. Iwaki, A. Shimizu, and C. Hotta, Thermal pure quantum matrix product states recovering a volume law entanglement, *Phys. Rev. Res.* **3**, L022015 (2021).

[45] S. Tsutsui, M. Hongo, S. Sato, and T. Sagawa, Quantum hydrodynamics from local thermal pure states, *Phys. Rev. Res.* **4**, 033059 (2022).

[46] M. Motta, C. Sun, A. T. Tan, M. J. O'Rourke, E. Ye, A. J. Minnich, F. G. Brandao, and G. K.-L. Chan, Determining eigenstates and thermal states on a quantum computer using quantum imaginary time evolution, *Nature Physics* **16**, 205 (2020).

[47] S. Lu, M. C. Bañuls, and J. I. Cirac, Algorithms for quantum simulation at finite energies, *PRX Quantum* **2**, 020321 (2021).

[48] C. Powers, L. B. Oftelie, D. Camps, and W. A. de Jong, Exploring finite temperature properties of materials with quantum computers (2022), [arXiv:2109.01619 \[quant-ph\]](https://arxiv.org/abs/2109.01619).

[49] L. Coopmans, Y. Kikuchi, and M. Benedetti, Predicting gibbs-state expectation values with pure thermal shadows, *PRX Quantum* **4**, 010305 (2023).

[50] A. Schuckert, A. Bohrtdt, E. Crane, and M. Knap, Probing finite-temperature observables in quantum simulators of spin systems with short-time dynamics, *Phys. Rev. B* **107**, L140410 (2023).

[51] A. Summer, C. Chiaracane, M. T. Mitchison, and J. Goold, Calculating the many-body density of states on a digital quantum computer, *Phys. Rev. Res.* **6**, 013106 (2024).

[52] E. Y. Loh, J. E. Gubernatis, R. T. Scalettar, S. R. White, D. J. Scalapino, and R. L. Sugar, Sign problem in the numerical simulation of many-electron systems, *Phys. Rev. B* **41**, 9301 (1990).

[53] M. Troyer and U.-J. Wiese, Computational complexity and fundamental limitations to fermionic quantum monte carlo simulations, *Phys. Rev. Lett.* **94**, 170201 (2005).

[54] A. Alexandru, G. Başar, P. F. Bedaque, and N. C. Warrington, Complex paths around the sign problem, *Rev. Mod. Phys.* **94**, 015006 (2022).

[55] S.-N. Sun, M. Motta, R. N. Tazhigulov, A. T. Tan, G. K.-L. Chan, and A. J. Minnich, Quantum computation of finite-temperature static and dynamical prop-

erties of spin systems using quantum imaginary time evolution, *PRX Quantum* **2**, 010317 (2021).

[56] L. Bassman, K. Klymko, D. Liu, N. M. Tubman, and W. A. de Jong, Computing free energies with fluctuation relations on quantum computers (2021), [arXiv:2103.09846 \[quant-ph\]](https://arxiv.org/abs/2103.09846).

[57] K. Yeter-Aydeniz, G. Siopsis, and R. C. Pooser, Scattering in the ising model with the quantum lanczos algorithm, *New Journal of Physics* **23**, 043033 (2021).

[58] K. Hémery, K. Ghanem, E. Crane, S. L. Campbell, J. M. Dreiling, C. Figgatt, C. Foltz, J. P. Gaebler, J. Johansen, M. Mills, S. A. Moses, J. M. Pino, A. Ransford, M. Rowe, P. Siegfried, R. P. Stutz, H. Dreyer, A. Schuckert, and R. Nigmatullin, Measuring the loschmidt amplitude for finite-energy properties of the fermi-hubbard model on an ion-trap quantum computer (2023), [arXiv:2309.10552 \[quant-ph\]](https://arxiv.org/abs/2309.10552).

[59] T. Jones, S. Endo, S. McArdle, X. Yuan, and S. C. Benjamin, Variational quantum algorithms for discovering hamiltonian spectra, *Phys. Rev. A* **99**, 062304 (2019).

[60] S. McArdle, T. Jones, S. Endo, Y. Li, S. C. Benjamin, and X. Yuan, Variational ansatz-based quantum simulation of imaginary time evolution, *npj Quantum Information* **5**, 75 (2019).

[61] X. Yuan, S. Endo, Q. Zhao, Y. Li, and S. C. Benjamin, Theory of variational quantum simulation, *Quantum* **3**, 191 (2019).

[62] S.-H. Lin, R. Dilip, A. G. Green, A. Smith, and F. Pollmann, Real- and imaginary-time evolution with compressed quantum circuits, *PRX Quantum* **2**, 010342 (2021).

[63] T. Liu, J.-G. Liu, and H. Fan, Probabilistic nonunitary gate in imaginary time evolution, *Quantum Information Processing* **20**, 204 (2021).

[64] N. Gomes, F. Zhang, N. F. Berthelsen, C.-Z. Wang, K.-M. Ho, P. P. Orth, and Y. Yao, Efficient step-merged quantum imaginary time evolution algorithm for quantum chemistry, *Journal of Chemical Theory and Computation* **16**, 6256 (2020), pMID: 32877181.

[65] K. Yeter-Aydeniz, R. C. Pooser, and G. Siopsis, Practical quantum computation of chemical and nuclear energy levels using quantum imaginary time evolution and lanczos algorithms, *npj Quantum Information* **6**, 63 (2020).

[66] K. Yeter-Aydeniz, E. Moschandreas, and G. Siopsis, Quantum imaginary-time evolution algorithm for quantum field theories with continuous variables, *Phys. Rev. A* **105**, 012412 (2022).

[67] H. Kamakari, S.-N. Sun, M. Motta, and A. J. Minnich, Digital quantum simulation of open quantum systems using quantum imaginary-time evolution, *PRX Quantum* **3**, 010320 (2022).

[68] A. Gilyén, Y. Su, G. H. Low, and N. Wiebe, Quantum singular value transformation and beyond: exponential improvements for quantum matrix arithmetics, in *Proceedings of the 51st Annual ACM SIGACT Symposium on Theory of Computing* (2019) pp. 193–204.

[69] J. M. Martyn, Z. M. Rossi, A. K. Tan, and I. L. Chuang, Grand unification of quantum algorithms, *PRX Quantum* **2**, 040203 (2021).

[70] G. H. Low and I. L. Chuang, Hamiltonian simulation by qubitization, *Quantum* **3**, 163 (2019).

[71] G. H. Low and I. L. Chuang, Optimal hamiltonian simulation by quantum signal processing, *Phys. Rev. Lett.* **118**, 010501 (2017).

[72] A. M. Childs and N. Wiebe, Hamiltonian simulation using linear combinations of unitary operations, *Quantum Info. Comput.* **12**, 901–924 (2012).

[73] D. W. Berry, A. M. Childs, R. Cleve, R. Kothari, and R. D. Somma, Exponential improvement in precision for simulating sparse hamiltonians, in *Proceedings of the Forty-Sixth Annual ACM Symposium on Theory of Computing*, STOC '14 (Association for Computing Machinery, New York, NY, USA, 2014) p. 283–292.

[74] D. W. Berry, A. M. Childs, and R. Kothari, Hamiltonian simulation with nearly optimal dependence on all parameters, in *2015 IEEE 56th Annual Symposium on Foundations of Computer Science* (2015) pp. 792–809.

[75] D. W. Berry, A. M. Childs, R. Cleve, R. Kothari, and R. D. Somma, Simulating hamiltonian dynamics with a truncated taylor series, *Phys. Rev. Lett.* **114**, 090502 (2015).

[76] G. H. Low, V. Kliuchnikov, and N. Wiebe, Well-conditioned multiproduct hamiltonian simulation (2019), [arXiv:1907.11679 \[quant-ph\]](https://arxiv.org/abs/1907.11679).

[77] E. T. Campbell, Early fault-tolerant simulations of the hubbard model, *Quantum Science and Technology* **7**, 015007 (2021).

[78] Y. Suzuki, S. Endo, K. Fujii, and Y. Tokunaga, Quantum error mitigation as a universal error reduction technique: Applications from the nisq to the fault-tolerant quantum computing eras, *PRX Quantum* **3**, 010345 (2022).

[79] L. Lin and Y. Tong, Heisenberg-limited ground-state energy estimation for early fault-tolerant quantum computers, *PRX Quantum* **3**, 010318 (2022).

[80] R. Kshirsagar, A. Katabarwa, and P. D. Johnson, On proving the robustness of algorithms for early fault-tolerant quantum computers (2022), [arXiv:2209.11322 \[quant-ph\]](https://arxiv.org/abs/2209.11322).

[81] Z. Ding and L. Lin, Even shorter quantum circuit for phase estimation on early fault-tolerant quantum computers with applications to ground-state energy estimation, *PRX Quantum* **4**, 020331 (2023).

[82] K. Kuroiwa and Y. O. Nakagawa, Clifford+ t -gate decomposition with limited number of t gates, its error analysis, and performance of unitary coupled cluster ansatz in pre-ftqc era (2023), [arXiv:2301.04150 \[quant-ph\]](https://arxiv.org/abs/2301.04150).

[83] Y. Akahoshi, K. Maruyama, H. Oshima, S. Sato, and K. Fujii, Partially fault-tolerant quantum computing architecture with error-corrected clifford gates and space-time efficient analog rotations, *PRX Quantum* **5**, 010337 (2024).

[84] P. K. Faehrmann, M. Steudtner, R. Kueng, M. Kieferova, and J. Eisert, Randomizing multi-product formulas for Hamiltonian simulation, *Quantum* **6**, 806 (2022).

[85] S. Chakraborty, Implementing any linear combination of unitaries on intermediate-term quantum computers (2023), [arXiv:2302.13555 \[quant-ph\]](https://arxiv.org/abs/2302.13555).

[86] A. Tosta, T. de Lima Silva, G. Camilo, and L. Aolita, Randomized semi-quantum matrix processing (2023), [arXiv:2307.11824 \[quant-ph\]](https://arxiv.org/abs/2307.11824).

[87] S. Wang, S. McArdle, and M. Berta, Qubit-efficient randomized quantum algorithms for linear algebra, *PRX Quantum* **5**, 020324 (2024).

[88] J. Peetz, S. E. Smart, and P. Narang, Quantum simulation via stochastic combination of unitaries (2024),

arXiv:2407.21095 [quant-ph].

[89] C. J. Geyer, Practical markov chain monte carlo, *Statistical Science* **7**, 473 (1992).

[90] W. Gilks, S. Richardson, and D. Spiegelhalter, *Markov Chain Monte Carlo in Practice*, Chapman & Hall/CRC Interdisciplinary Statistics (CRC Press, 1995).

[91] M. K. Cowles and B. P. Carlin, Markov chain monte carlo convergence diagnostics: A comparative review, *Journal of the American Statistical Association* **91**, 883 (1996).

[92] S. Brooks, Markov chain monte carlo method and its application, *Journal of the Royal Statistical Society: Series D (The Statistician)* **47**, 69 (1998).

[93] J. C. Getelina, N. Gomes, T. Iadecola, P. P. Orth, and Y.-X. Yao, Adaptive variational quantum minimally entangled typical thermal states for finite temperature simulations, *SciPost Phys.* **15**, 102 (2023).

[94] K. Pollock, P. P. Orth, and T. Iadecola, Variational microcanonical estimator, *Phys. Rev. Res.* **5**, 033224 (2023).

[95] J. Gacon, J. Nys, R. Rossi, S. Woerner, and G. Carleo, Variational quantum time evolution without the quantum geometric tensor, *Phys. Rev. Res.* **6**, 013143 (2024).

[96] Y. Shen, K. Klymko, E. Rabani, D. Camps, R. V. Beeumen, and M. Lindsey, Efficient quantum trace estimation with reconfigurable real-time circuits (2024), arXiv:2401.04176 [quant-ph].

[97] W. Qian and B. Wu, Quantum computation in fermionic thermal field theories (2024), arXiv:2404.07912 [hep-ph].

[98] A. M. Childs, R. Kothari, and R. D. Somma, Quantum algorithm for systems of linear equations with exponentially improved dependence on precision, *SIAM Journal on Computing* **46**, 1920 (2017).

[99] T. Loke and J. Wang, Efficient quantum circuits for szegedy quantum walks, *Annals of Physics* **382**, 64 (2017).

[100] D. Camps and R. Van Beeumen, Fable: Fast approximate quantum circuits for block-encodings, in *2022 IEEE International Conference on Quantum Computing and Engineering (QCE)* (2022) pp. 104–113.

[101] D. Camps, L. Lin, R. V. Beeumen, and C. Yang, Explicit quantum circuits for block encodings of certain sparse matrices (2023), arXiv:2203.10236 [quant-ph].

[102] M. Abramowitz and I. Stegun, *Handbook of Mathematical Functions with Formulas, Graphs, and Mathematical Tables*, Applied mathematics series (U.S. Government Printing Office, 1964).

[103] C. Marteau, Ground state preparation via qubitization (2023), arXiv:2306.14993 [quant-ph].

[104] D. Poulin and P. Wocjan, Sampling from the thermal quantum gibbs state and evaluating partition functions with a quantum computer, *Phys. Rev. Lett.* **103**, 220502 (2009).

[105] A. N. Chowdhury and R. D. Somma, Quantum algorithms for gibbs sampling and hitting-time estimation, *Quantum Info. Comput.* **17**, 41–64 (2017).

[106] J. van Apeldoorn, A. Gilyén, S. Gribling, and R. de Wolf, Quantum SDP-Solvers: Better upper and lower bounds, *Quantum* **4**, 230 (2020).

[107] T. L. Silva, M. M. Taddei, S. Carrazza, and L. Aolita, Fragmented imaginary-time evolution for early-stage quantum signal processors, *Scientific Reports* **13**, 18258 (2023).

[108] A. N. Chowdhury, R. D. Somma, and Y. Subaş 1, Computing partition functions in the one-clean-qubit model, *Phys. Rev. A* **103**, 032422 (2021).

[109] S. Sachdeva and N. Vishnoi, Approximation theory and the design of fast algorithms (2013), arXiv:1309.4882 [cs.DS].

[110] A. Barenco, C. H. Bennett, R. Cleve, D. P. DiVincenzo, N. Margolus, P. Shor, T. Sleator, J. A. Smolin, and H. Weinfurter, Elementary gates for quantum computation, *Phys. Rev. A* **52**, 3457 (1995).

[111] M. Nielsen and I. Chuang, *Quantum Computation and Quantum Information*, Cambridge Series on Information and the Natural Sciences (Cambridge University Press, 2000).

[112] Y. Suzuki, Y. Kawase, Y. Masumura, Y. Hiraga, M. Nakadai, J. Chen, K. M. Nakanishi, K. Mitarai, R. Imai, S. Tamiya, T. Yamamoto, T. Yan, T. Kawakubo, Y. O. Nakagawa, Y. Ibe, Y. Zhang, H. Yamashita, H. Yoshimura, A. Hayashi, and K. Fujii, Qulacs: a fast and versatile quantum circuit simulator for research purpose, *Quantum* **5**, 559 (2021).

[113] W. Hoeffding, Probability inequalities for sums of bounded random variables, *Journal of the American Statistical Association* **58**, 13 (1963).

[114] M. H. Quenouille, Approximate tests of correlation in time-series, *Journal of the Royal Statistical Society. Series B (Methodological)* **11**, 68 (1949).

[115] M. H. Quenouille, NOTES ON BIAS IN ESTIMATION, *Biometrika* **43**, 353 (1956).

[116] J. W. Tukey, Bias and confidence in not quite large samples, *The Annals of Mathematical Statistics* **29**, 614 (1958).

[117] B. Efron and R. Tibshirani, *An Introduction to the Bootstrap*, Chapman & Hall/CRC Monographs on Statistics & Applied Probability (Taylor & Francis, 1994).

[118] S. Endo, S. C. Benjamin, and Y. Li, Practical quantum error mitigation for near-future applications, *Phys. Rev. X* **8**, 031027 (2018).

[119] T. P. Harty, D. T. C. Allcock, C. J. Ballance, L. Guidoni, H. A. Janacek, N. M. Linke, D. N. Stacey, and D. M. Lucas, High-fidelity preparation, gates, memory, and readout of a trapped-ion quantum bit, *Phys. Rev. Lett.* **113**, 220501 (2014).

[120] R. Srinivas, S. Burd, H. Knaack, R. Sutherland, A. Kwiatkowski, S. Glancy, E. Knill, D. Wineland, D. Leibfried, A. C. Wilson, *et al.*, High-fidelity laser-free universal control of trapped ion qubits, *Nature* **597**, 209 (2021).

[121] C. R. Clark, H. N. Tinkey, B. C. Sawyer, A. M. Meier, K. A. Burkhardt, C. M. Seck, C. M. Shappert, N. D. Guise, C. E. Volin, S. D. Fallek, H. T. Hayden, W. G. Rellergert, and K. R. Brown, High-fidelity bell-state preparation with $^{40}\text{Ca}^+$ optical qubits, *Phys. Rev. Lett.* **127**, 130505 (2021).

[122] S. A. Moses, C. H. Baldwin, M. S. Allman, R. Ancona, L. Ascarrunz, C. Barnes, J. Bartolotta, B. Bjork, P. Blanchard, M. Bohn, J. G. Bohnet, N. C. Brown, N. Q. Burdick, W. C. Burton, S. L. Campbell, J. P. Campora, C. Carron, J. Chambers, J. W. Chan, Y. H. Chen, A. Chernoguzov, E. Chertkov, J. Colina, J. P. Curtis, R. Daniel, M. DeCross, D. Deen, C. Delaney, J. M. Dreiling, C. T. Ertsgaard, J. Esposito, B. Estey, M. Fabrikant, C. Figgatt, C. Foltz, M. Foss-Feig, D. Francois, J. P. Gaebler, T. M. Gatterman,

C. N. Gilbreth, J. Giles, E. Glynn, A. Hall, A. M. Han-kin, A. Hansen, D. Hayes, B. Higashi, I. M. Hoffman, B. Horning, J. J. Hout, R. Jacobs, J. Johansen, L. Jones, J. Karcz, T. Klein, P. Lauria, P. Lee, D. Liefer, S. T. Lu, D. Lucchetti, C. Lytle, A. Malm, M. Matheny, B. Mathewson, K. Mayer, D. B. Miller, M. Mills, B. Neyenhuis, L. Nugent, S. Olson, J. Parks, G. N. Price, Z. Price, M. Pugh, A. Ransford, A. P. Reed, C. Roman, M. Rowe, C. Ryan-Anderson, S. Sanders, J. Sedlacek, P. Shevchuk, P. Siegfried, T. Skripka, B. Spaun, R. T. Sprenkle, R. P. Stutz, M. Swallows, R. I. Tobey, A. Tran, T. Tran, E. Vogt, C. Volin, J. Walker, A. M. Zolot, and J. M. Pino, A race-track trapped-ion quantum processor, *Phys. Rev. X* **13**, 041052 (2023).

[123] M. P. da Silva, C. Ryan-Anderson, J. M. Bello-Rivas, A. Chernoguzov, J. M. Dreiling, C. Foltz, F. Fra-
chon, J. P. Gaebler, T. M. Gatterman, L. Grans-
Samuelsson, D. Hayes, N. Hewitt, J. Johansen, D. Lucchetti, M. Mills, S. A. Moses, B. Neyenhuis, A. Paz, J. Pino, P. Siegfried, J. Strabley, A. Sundaram, D. Tom, S. J. Wernli, M. Zanner, R. P. Stutz, and K. M. Svore, Demonstration of logical qubits and repeated error correction with better-than-physical error rates (2024), [arXiv:2404.02280 \[quant-ph\]](https://arxiv.org/abs/2404.02280).

[124] G. Brassard, P. Hoyer, M. Mosca, and A. Tapp, Quantum amplitude amplification and estimation, *Contemporary Mathematics* **305**, 53 (2002).

[125] A. Gelman and D. B. Rubin, Inference from Iterative Simulation Using Multiple Sequences, *Statistical Science* **7**, 457 (1992).

[126] A. Gelman, J. Carlin, H. Stern, and D. Rubin, *Bayesian Data Analysis*, Chapman & Hall/CRC Texts in Statistical Science (Chapman & Hall/CRC, 2003).

[127] D. Vats and C. Knudson, Revisiting the Gelman-Rubin Diagnostic, *Statistical Science* **36**, 518 (2021).